University of Alberta

Calculations of Electron Transport through Substituted Benzenes

by

Manuel Smeu

A thesis submitted to the Faculty of Graduate Studies and Research
in partial fulfillment of the requirements for the degree of

Master of Science

Department of Physics

Edmonton, Alberta
Fall 2007

Library and Archives Canada

Published Heritage Branch

395 Wellington Street
Ottawa ON K1A 0N4
Canada

Bibliothèque et Archives Canada

Direction du Patrimoine de l'édition

395, rue Wellington
Ottawa ON K1A 0N4
Canada

Your file Votre référence
ISBN: 978-0-494-33353-2
Our file Notre référence
ISBN: 978-0-494-33353-2

NOTICE:
The author has granted a non-exclusive license allowing Library and Archives Canada to reproduce, publish, archive, preserve, conserve, communicate to the public by telecommunication or on the Internet, loan, distribute and sell theses worldwide, for commercial or non-commercial purposes, in microform, paper, electronic and/or any other formats.

The author retains copyright ownership and moral rights in this thesis. Neither the thesis nor substantial extracts from it may be printed or otherwise reproduced without the author's permission.

AVIS:
L'auteur a accordé une licence non exclusive permettant à la Bibliothèque et Archives Canada de reproduire, publier, archiver, sauvegarder, conserver, transmettre au public par télécommunication ou par l'Internet, prêter, distribuer et vendre des thèses partout dans le monde, à des fins commerciales ou autres, sur support microforme, papier, électronique et/ou autres formats.

L'auteur conserve la propriété du droit d'auteur et des droits moraux qui protège cette thèse. Ni la thèse ni des extraits substantiels de celle-ci ne doivent être imprimés ou autrement reproduits sans son autorisation.

In compliance with the Canadian Privacy Act some supporting forms may have been removed from this thesis.

While these forms may be included in the document page count, their removal does not represent any loss of content from the thesis.

Conformément à la loi canadienne sur la protection de la vie privée, quelques formulaires secondaires ont été enlevés de cette thèse.

Bien que ces formulaires aient inclus dans la pagination, il n'y aura aucun contenu manquant.

Canada

Abstract

Electron transport through disubstituted benzenedithiol (BDT) molecules bridging two electrodes was modeled using a combination of density functional theory and a non-equilibrium Green's function technique. For Au electrodes of 3x3 atomic cross-section, the BDT's with the electron donating groups (EDG) had higher conductance than those with electron withdrawing groups (EWG). The highest occupied molecular orbital contributes to transmission and it gets shifted closer to the Fermi level of the electrodes by EDG's. The conductance showed an excellent linear correlation with the substituent parameter σ_p and displayed negative differential resistance (NDR). The correlation and NDR were not found for electrodes of 5x5 cross-section showing they were due to the small size of the 3x3 electrodes. When Al electrodes of 3x3 cross-section were used, a qualitatively different behaviour was found, the highest conductance was calculated for the benzenedithiols containing weak EWG's. An unoccupied molecular orbital was responsible for the transmission in this case.

Acknowledgement

I would like to express my gratitude to Gino DiLabio and Robert Wolkow for supervising the work for this thesis. I have learned so much over the last two years from these individuals and the lessons will not be forgotten. Both Gino and Bob have always made time for me without hesitation despite their busy schedules. They continue to be helpful with my transition to the next stage and I truly appreciate it. I am indebted to Hong Guo and Derek Waldron for providing the MATDCAL code and the invaluable technical assistance. I would also like to thank my family for always encouraging me to do my best. Their love and support are what kept me motivated. Finally, I want to thank Avenelle Johnson for being so understanding and supportive. There were countless times when it felt hopeless and I was overwhelmed with stress but she would always keep a positive attitude and reassure me that I will get it done.

Table of Contents

1 Introduction **1**

2 Theory **11**

2.1 Schrödinger Equation and Density Functional Theory 12

2.1.1 The Schrödinger Equation 12

2.1.2 Born-Oppenheimer Approximation 15

2.1.3 Exchange and Correlation 16

2.1.4 DFT: Hohenberg-Kohn Theorem 16

2.1.5 DFT: Kohn-Sham Equations 17

2.1.6 Local-Density Approximation 21

2.1.7 Basis Sets 23

2.1.8 Pseudopotentials 26

2.2 Landauer-Büttiker Theory 26

2.2.1 Reflectionless Contacts 28

2.2.2 Transmission and Reflection 30

2.3 Non-Equilibrium Green's Function 31

2.3.1 Model of the System 31

2.3.2 Non-Equilibrium Green's Function 32

2.3.3 Determining the self-energy Σ 36

3 Computational methods **38**

3.1 Geometry optimizations 38

3.2 MATDCAL calculations 41

3.2.1 Basis sets 42

3.2.2 Bulk calculations 42

3.2.3 Two-probe systems 46

4 Results and Discussion **51**

4.1 The Au-BDT-Au system 51

4.2 Transport through the 3x3 Au-BDT-Au system 55

4.3 The effect of substituent groups on transport through the 3x3 Au-BDT-Au system 65

4.4 Transport through the 5x5 Au-BDT-Au system 78

4.5 The substituted 3x3 Al-BDT-Al system 83

5 Conclusions 90

Bibliography 93

Appendix A 101

Appendix B 104

List of Tables

Table 3.1. The parameters used for the electrodes in the three systems studied. The dimensions of the cell in the x and y directions are made larger so that images do not interact. At least 3 grid points were used per a. u. along each direction. Only one k-point was needed along the x and y axes since images did not interact in those directions, but 10 k-points were used in the z-direction since interactions in this direction are important to properly model a nanowire 45

Table 3.2. The parameters used for the scattering region in the three systems studied. The dimensions of the cell in the x and y directions are made larger so that images are too far apart to interact in these directions. At least 3 grid points were used per a.

u. along each direction. Only one k-point was needed in the x and y-directions since images did not interact in those directions and there was no value for k-points in the z-direction since the scattering region is not periodic in this direction 49

Table 4.1. Position of the HOMO and LUMO+2 levels for the 11 substituted 4Au-BDT-4Au systems. The Hammett substituent constant σ_p which is a measure of the strength of a group as an EDG/EWG is also included. The EDG's are at the top of the table and the EWG's are at the bottom. 74

List of Figures

Figure 1.1. Model of a molecule or nanoparticle bridging two metallic electrodes. As a bias is applied to the electrodes a resulting current will pass through the molecule or nanoparticle.. 3

Figure 1.2. Model of a molecule bridging two electrodes. The system is divided into three regions: a left electrode, a scattering region and a right electrode. 7

Figure 1.3. A schematic representation of benzenedithiol (a), a molecular structure of benzenedithiol (b) and a molecular structure of benzenedithiol bonded to two Au electrodes (c). 8

Figure 2.1. Dispersion relation for a single one-dimensional subband. The $+k$ states are on the positive k-axis and filled up to μ_1 while the $-k$ states are on the negative k-axis and filled up to μ_2. In terms of current, the $+k$ and $-k$ states below μ_2 essentially cancel out so that

only the $+k$ states between μ_1 and μ_2 need to be considered (blue shaded region). 29

Figure 2.2. The system studied consists of a scattering region containing the molecule of interest as well as several layers of each lead and semi-infinite left and right leads. 32

Figure 2.3. Self-consistent cycle between the DFT and NEGF calculations. The density is used to calculate the Hamiltonian in DFT. This Hamiltonian is then used along with the self-energies and the electrochemical potentials in order to calculate the density matrix in NEGF. This density matrix is used in the following DFT calculation and the cycle is repeated until self-consistency is achieved. 35

Figure 3.1. The 4Au-BDT-4Au structure used for the geometry optimization. The positions of the Au atoms are held fixed to their bulk positions with the exception that the plane-plane separation was allowed to relax. The entire BDT molecule was allowed to relax. 39

Figure 3.2. The Au-BDT-Au systems used in the calculations. The BDT structure and the electrode-electrode separation were optimized. Au atoms were then added to their bulk crystal positions. The top

left and right schematics show the 3x3 Au-BDT-Au system from side and end views, respectively; the bottom left and right schematics show the 5x5 Au-BDT-Au system from side and end views, respectively. 41

Figure 3.3. A supercell with 8 of its images which show the periodicity. This setup is used to model a nanowire; by including a vacuum region in the x and y-directions there is no interaction between the images in those directions. The cell is repeated infinitely in the x, y and z-directions. 43

Figure 3.4. A two-probe system and two of its images in the y-direction consisting of a scattering region between left and right electrodes. The electrodes are semi-infinite and the entire structure is repeated in the x and y-directions. 47

Figure 4.1. The atomic arrangement of the first two layers of an Au (100) surface along with the positions of the hollow site (A), top site (B) and bridge site (C) where a S atom can bind. 54

Figure 4.2. Transmission spectrum and DOS for the 3x3 Au-BDT-Au system at zero bias. The position of the eigenstates from the 4Au-BDT-4Au molecule are shown at the top: (o) for σ-type MO's and

(x) for π-type MO's. The energy scale is relative to the Fermi level of the electrodes (-3.84 eV). 56

Figure 4.3. DOS (top) and transmission spectra (bottom) for the 3x3 Au-BDT-Au system for different biases applied to the right electrode. The energy is relative to the Fermi level of the left electrode which was at -3.84 eV. 59

Figure 4.4. I-V plot for the 3x3 Au-BDT-Au system shown in Fig 3.2. . 63

Figure 4.5. Substituted BDT system used. The substituent groups span a range from the electron donating $N(CH_3)_2$ to the electron withdrawing NO_2. For each system the two R groups would be the same. 66

Figure 4.6. DOS (top) and transmission spectra (bottom) relative to the Fermi level of the electrodes (-3.84 eV) for three different substituents at zero bias including the EDG NH_2 and EWG NO_2. The positions of the π-type MO's of the 4Au-BDT-4Au molecule are shown at the top for each system. 67

Figure 4.7. a) The scattering state for the unsubstituted (R=H) 3x3 Au-BDT-Au system in Fig. 4.6 at the peak of the transmission curve (-0.08 eV). b) The HOMO of the 4Au-BDT-4Au system shown in c). Note the resemblance between the scattering state and the HOMO

which confirms that transmission peak is due to conductance through the HOMO level. 71

Figure 4.8. A scattering state showing reflection for the unsubstituted (R=H) 3x3 Au-BDT-Au system in Fig. 4.6 at -0.3 eV, where the transmission is close to zero. 72

Figure 4.9. Molecular orbitals of unsubstituted 4Au-BDT-4Au that are close to the Fermi level in the Au-BDT-Au system. The HOMO and LUMO+2 MO's are π-type orbitals with a nodal plane on the plane formed by the benzene ring. The LUMO and LUMO+1 MO's are σ-type orbitals. 73

Figure 4.10. I-V characteristics for the 3x3 Au-BDT-Au system with different substituents. BDT with ED substituents has a higher current at a given bias than BDT with EW substituents. 76

Figure 4.11. Correlation between transmission at the Fermi level for zerobias and the Hammett substituent constant σ_p for the 3x3 Au-BDT-Au system 77

Figure 4.12. Transmission spectra for the 5x5 Au-BDT-Au system shown in Fig 3.2 with different substituents. The energy scale is relative to the Fermi level (-3.62 eV). 79

Figure 4.13. I-V comparison of current as a function of bias for three representative substituents with the small (3x3) and large (5x5) electrodes. There is no manifestation of NDR for the systems with 5x5 electrodes. The ordering of the curves is the same for the systems with both the small and large electrodes: systems with the NH_2 substituent have a slightly higher current than unsubstituted systems, which have a much higher current than systems substituted with NO_2. 82

Figure 4.14. DOS for the Al-BDT-Al system for molecules with three different substituents: NH_2, H, and COOH. The relative positioning of the σ-type (o) and π-type (x) MO's of the 4Al-BDT-4Al molecule are shown at the top. The energy scale is relative to the Fermi level for Al 3x3 electrodes: -3.93 eV. 84

Figure 4.15. The transmission as a function of energy relative to the Fermi level (-3.92 eV) for the 3x3 Al-BDT-Al systems with different substituents on the molecule. Top: substituents are EDG's; Bottom: substituents are EWG's. The relative positions of the MO's for the COOH substituted 4Al-BDT-4Al molecule: (o) for σ-type and (x) for π-type. 86

Figure 4.16. A comparison of a) the scattering state for the COOH

substituted 3x3 Al-BDT-Al system in Fig. 4.15 at the peak of the transmission curve (0.16 eV) with b) the LUMO+1 of the COOH substituted 4Al-BDT-4Al molecule shown in c). 88

Figure 4.17. I-V plot for the 3x3 Al-BDT-Al system for BDT molecules containing different substituent groups. 89

Abbreviations

BDT	benzenedithiol
DFT	density functional theory
DOS	density of states
EDG	electron donating group
EWG	electron withdrawing group
GGA	generalized gradient approximation
HK	Hohenberg-Kohn
HOMO	highest occupied molecular orbital
I-V	current-voltage
LCAO	linear combination of atomic orbitals
LDA	local density approximation
LUMO	lowest unoccupied molecular orbital
MO	molecular orbital

NEGF	non-equilibrium Green's function
PS	pseudopotential
QSAR	quantitative structure activity relationship
SE	Schrödinger equation
STM	scanning tunneling microscopy

Chapter 1

Introduction

As the size of electronics approaches the physical limits of CMOS technology, a clear understanding of their operating features at the nanoscale must be achieved. The size limits of electronic components will be reached because quantum effects begin to play an important role in structures on the size scale of several tens of nanometers. This size scale is known as the mesoscopic regime where classical laws of electricity such as Ohm's law no longer hold. In this regime the size of the device is comparable to, or smaller than, the de Broglie wavelength of the electron.

It has been suggested that organic molecules can be used as replacements to or in conjunction with conventional CMOS technology [1, 2]. The pioneering work in this area was made by Aviram and Ratner who

showed that, in principle, a single molecule can act as a rectifier [3]. This prediction was verified experimentally 25 years later by Metzger *et al.* [4, 5] when a zwitterionic molecule sandwiched between two electrodes gave evidence for electrical rectification. With the use of scanning tunnelling microscopy (STM), Piva *et al.* [6] demonstrated the ability to regulate the conductivity of a single molecule bound to silicon with an electric field emanating from a nearby charged dangling bond on the surface. These are just two examples of the progress that has been made in the development of basic electronic devices from molecules. One of the reasons why organic molecules are the prime candidates in the development of molecular electronic devices is because their properties can be widely varied and specifically tuned in order to design a molecule with desired electronic properties. Additionally, the chemical reactions used to make them are well understood and can often be subjected to self-assembly so that the product yields can be well controlled.

Studies in this area predominantly use the model of a molecule (or nanoparticle) bridging two electrodes (Fig. 1.1). The application of an electrical bias to one of the electrodes in this model would result in an electrochemical potential drop across the molecule and an electrical current passing through it.

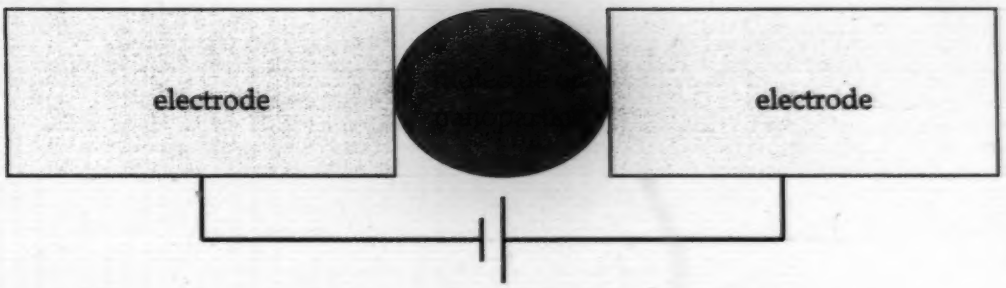

Figure 1.1. Model of a molecule or nanoparticle bridging two metallic electrodes. As a bias is applied to the electrodes a resulting current will pass through the molecule or nanoparticle.

The experimental work in this area has been mainly dominated by two techniques of measuring an electrical current passing through a molecule bridging two electrodes under a finite bias. These are mechanically-controlled break junction experiments and STM.

Mechanically-controlled break junction experiments [7] involve a piece of conducting material being broken into two pieces as a result of a force applied by a piezoelectric crystal. The separation between the two pieces of the broken conductor can then be very precisely controlled with the application of a voltage to the piezoelectric crystal. Molecules of interest can be arranged to bridge the gap between the two pieces, and their electrical properties can be observed by running a current through them (for examples see ref. [8]). One shortcoming of this technique is that one lacks the knowledge of what is being measured in the gap, namely the

identity and the number of molecules. Additionally, since the conductor was broken, the exact structure in the gap is not known and the geometry at the interfaces is not consistent from one experiment to the next.

In STM, a surface is imaged by measuring the tunneling current between it and a scanning tip. The tip can also be held in a particular position over the sample and the current-voltage (I-V) properties can be measured. Molecules attached to the surface via covalent bonds can also be studied in this manner (see, for example, ref. [9]). In this case the surface acts as one electrode while the tip acts as the other and the tunneling current through the molecule can be measured. The appeal of this technique is that the sample can be imaged before and after measurements so that one has a good idea of what is being measured. However, since the measurements are of a tunneling current, it is not straightforward to relate the results to a model where the molecule is covalently bonded to both electrodes, which is desirable for a molecular electronic device.

Another approach to experimental measurements of conductance through a single molecule is a combination of the two techniques mentioned above [10, 11]. A modified STM is used in which the tip is actually crashed into the surface in order to make a point contact. In the

presence of a solution containing the molecules of interest, the tip is then pulled away from the surface, so the point contact is broken, and that one or more molecules can be trapped between the tip and the surface. A great advantage of this procedure is that it can be automated to be repeated several thousands of times in order to obtain detailed statistical analyses of the I-V characteristics from various possible binding arrangements between the molecules and the electrodes [10].

There have also been substantial developments in the first-principles treatment of molecules between two electrodes. For example, the Landauer-Büttiker [12] formalism has been very useful in the study of quantum transport [13]. In the Landauer-Büttiker picture, the electrode-molecule-electrode model is used in such a way that an electron passing from one electrode, through the molecule, to the other electrode can only experience reflections in the molecule itself (not in the electrodes). The current is then simply given by the probability that an electron will be transmitted through (not reflected by) the molecule.

Several theoretical approaches have made use of the Landauer-Büttiker formalism. They include semi-empirical methods, supercell methods and open jellium methods. The drawback of using the semi empirical methods [14, 15, 16, 17] is that they use parametrized

Hamiltonians which are derived from isolated molecular calculations for the molecule part of the system, and bulk calculations for the electrode parts of the system. It has been shown that this approach is not always reliable for modeling the coupling of a molecular system to a bulk system since they received different treatments [18]. The supercell methods [19, 20, 21, 22] use periodic boundary conditions to solve the Kohn-Sham equations [23]. However, because of the periodic boundary conditions necessary for the calculations, these methods are limited to periodic systems and calculations of systems with an external bias are not possible. The open jellium lead methods [24, 25, 26, 27, 28] use electrodes described as a uniformly charged compensating background. The drawback of this technique is that only low bias conditions can be treated with a reasonable degree of accuracy due to the electronic structure of the leads not being taken into account.

An approach has been developed [18, 29, 30] that accounts for the limitations of the treatments mentioned above. This method has been implemented as a MATLAB program which is called MATDCAL [30]. It uses a combination of density functional theory (DFT) and a non-equilibrium Green's function (NEGF) technique to perform electron transport calculations. The system is divided into three regions: left and

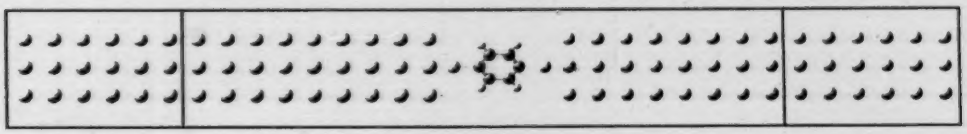

Figure 1.2. Model of a molecule bridging two electrodes. The system is divided into three regions: a left electrode, a scattering region and a right electrode.

right electrodes, and a scattering region (Fig. 1.2). The electrodes are not constrained to be the same and open systems (under an external bias) can also be treated. Separate periodic calculations are performed on each electrode, from which the self-energies of the electrodes can be obtained. The charge density can then be calculated inside the finite scattering region by including the effect of the electrodes as self-energies via a Green's function technique. This effectively reduces an infinite problem to one of finite size where the explicit structure of the leads is included as well as allowing for an external bias.

Although the results from early theoretical and experimental studies on these two probe systems differed by many orders of magnitude, recent advances in theoretical methods as well as a deeper understanding of experimental binding geometries of the molecule to the leads has closed the gap between the two substantially [31, 32, 33]. The

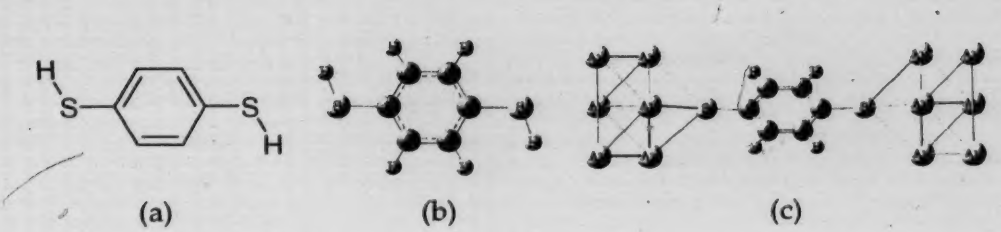

Figure 1.3. A schematic representation of benzenedithiol (a), a molecular structure of benzenedithiol (b) and a molecular structure of benzenedithiol bonded to two Au electrodes (c).

conductance of a large number of systems between theory and experiment agrees to within one order of magnitude. However there remain some puzzling cases in which a large difference between the two persists [32]. An example of such a molecule is benzenedithiol (BDT, Fig 1.3).

Electron transport through BDT has received much attention both experimentally and theoretically. Its popularity stems from its simplicity compared to other conducting molecules, the high binding affinity that the thiol group has for gold surfaces as well as its π molecular orbitals (MO) that facilitate electron transport due to their delocalized nature. There remains a lack of consistent conductance data between experiment and theory (and even between separate experiments [34] or different calculations [32]) despite the popularity of this molecule in many studies. One explanation given for this is that the S atom can have many different

favourable binding configurations to the Au electrode [32]. Slight changes in the configuration and even in the conformation of the molecule can result in a drastic change in conductance [35, 36, 37, 38]. Additionally, since the BDT molecule is so small, this makes experimental measurements on it relatively difficult. It is also not well understood how the structural distortion of the molecule due to a current passing through it and the presence of an electric field affects its electrical properties. However this aspect is not considered in this work and is assumed to play a relatively minor role at low bias and current.

In this thesis, electron transport through the BDT molecule bridging Au electrodes of finite cross section was studied in order to gain a better understanding of this system. The MATDCAL package was used for the calculations that employ DFT with the NEGF formalism. A variety of chemical groups were substituted onto BDT in order to assess how changes in the electronic structure of the molecule alter conductance. This will also give some insight into how current flow can be tuned by judiciously selecting the molecule that is used. Electrodes of differing cross-sectional area (3x3 vs. 5x5) and different elemental composition (Au vs. Al) were also compared.

The organization of this thesis is as follows. In Chapter 2, a brief summary of the theory used for this work, including density functional theory (DFT) as well as Landauer-Büttiker theory and the non-equilibrium Green's function (NEGF) formalism, are presented. In Chapter 3, the computational methods that were used for the calculations are described. The Gaussian 03 [39] package was used for geometry optimizations while MATDCAL [30] was used for the electron transport calculations. In Chapter 4, the results for conductance of substituted BDT molecules are presented and discussed. Electrodes of differing cross-sectional area and different elements are also compared. A brief summary is given in Chapter 5.

Chapter 2

Theory

This chapter outlines the theoretical methods used in this work. It is divided into three sections: Schrödinger Equation and Density Functional Theory, Landauer-Büttiker Theory, and Non-Equilibrium Green's Function formalism.

In the first section, the Schrödinger equation is introduced along with some of the difficulties involved in solving it. Some popular approximations are also discussed. The Hohenberg-Kohn theorem and Kohn-Sham equations used in density functional theory (DFT) are outlined as well as the local density approximation (LDA) which is used for the exchange-correlation energy functional. The second section outlines the Landauer-Büttiker theory for modeling electron transport at

the nanoscale by obtaining the current from the probability of an electron transmitting through the molecule. The last section of this chapter presents the equations used in the non-equilibrium Green's function (NEGF) formalism which permit the calculation for the transmission function of a system. The self-consistent relationship between the NEGF approach and DFT is also discussed.

2.1 Schrödinger Equation and Density Functional Theory

More in-depth information on the following three sub-sections can be found in ref. [40], or in any other good Quantum Mechanics textbook.

2.1.1 The Schrödinger Equation

The Schrödinger equation (SE) describes the space- and time-dependence of quantum mechanical systems. Once defined for a particular system, it contains all of the information about that system that can be known. The treatment in this work deals with the non-relativistic time-independent SE,

$$\hat{H}\Psi\left(\left\{\vec{x}_i, \vec{R}_I\right\}\right) = E\Psi\left(\left\{\vec{x}_i, \vec{R}_I\right\}\right) \tag{2.1}$$

with $\Psi\left(\{\vec{x}_i, \vec{R}_I\}\right)$ being the wave function where $\vec{x}_i = (\vec{r}_i, s_i)$, $\vec{r}_i$ are the spatial coordinates and s_i being the spin coordinate for electron i out of a total of N_e electrons, and $\vec{R}_I$ being the spatial coordinates for nucleus I out of a total of N_N nuclei. $\hat{H}$, the Hamiltonian of the system, is the observable corresponding to the total energy E of the system and it is given as a sum of the kinetic energy of the electrons, the Coulombic electron-nucleus attraction, the Coulombic electron-electron repulsion, the kinetic energy of the nuclei, and the Coulombic nucleus-nucleus repulsion,

$$\hat{H} = \hat{T}_e + \hat{V}_{eN} + \hat{U} + \hat{T}_N + \hat{V}_{NN}. \tag{2.2}$$

By using atomic units ($e = m_e = \hbar = 1$), the kinetic energy of the electrons is given as

$$\hat{T}_e = -\frac{1}{2}\sum_i \nabla_i^2 \tag{2.3}$$

where the summation runs over all electrons i and ∇ is the derivative in space. The Coulombic electron-nucleus attraction is given as

$$\hat{V}_{eN} = \sum_{i,I} \frac{Z_I}{|\vec{r}_i - \vec{R}_I|} \tag{2.4}$$

where the summation runs over all electrons and nuclei. Z_I and $\vec{R}_I$ are the atomic number and coordinates for nucleus I, and $\vec{r}_i$ are the

coordinates for electron i. The Coulombic electron-electron repulsion is given as

$$\hat{U} = \frac{1}{2}\sum_{i \neq j} \frac{1}{|\vec{r}_i - \vec{r}_j|} \tag{2.5}$$

where the summation runs over all electron pairs (the factor ½ is added to compensate for each pair being included twice). $\vec{r}_i$ and $\vec{r}_j$ are the coordinates for electrons i and j. The kinetic energy of the nuclei is given as

$$\hat{T}_N = -\sum_I \frac{1}{2M_I} \nabla_I^2 \tag{2.6}$$

where the summation runs over all nuclei and M_I is the mass of nucleus I. The Coulombic nucleus-nucleus repulsion is given as

$$\hat{V}_{NN} = \frac{1}{2}\sum_{I \neq J} \frac{Z_I Z_J}{|\vec{R}_I - \vec{R}_J|} \tag{2.7}$$

where the summation runs over all nucleus pairs. Z_I, Z_J are the charges and $\vec{R}_I$, $\vec{R}_J$ are the coordinates for nuclei I and J.

Equation (2.1) is a many-body problem which is impossible to solve exactly for more than one electron. For this reason, many approximations can be made to reduce this to a problem that can be solved computationally. Some of these approximations are outlined below.

2.1.2 Born-Oppenheimer Approximation

The Born-Oppenheimer approximation (or adiabatic approximation) simplifies the SE with the assumption that the nuclei can be treated as being stationary. This is valid in many cases because the mass of a nucleus is much greater than the mass of an electron and it is assumed that electrons will instantaneously relax with respect to the positions of the nuclei whose effect can be included as an external field $\hat{V}_{ext}$. Equation (2.1) can be separated into an electronic and a nuclear part, and the latter is treated independently. The kinetic and potential energies of the nuclei can be added in after the electronic SE has been solved. The SE can now be written as

$$\hat{H}_{elec}\Psi_{elec}(\vec{x}_i) = [\hat{T}_e + \hat{U} + \hat{V}_{ext}]\Psi_{elec}(\vec{x}_i) = E_{elec}\Psi_{elec}(\vec{x}_i) \tag{2.8}$$

where the subscript *elec* is included to emphasize that this is not the full SE. $\hat{T}_N$ and $\hat{V}_{NN}$ are removed and $\hat{V}_{eN}$ is replaced with $\hat{V}_{ext}$ to emphasize the fact that the electrons move under the influence of the nuclei as to an external field. From here on, the subscript *elec* will not be included, but the following discussion about the SE does refer to Eq. (2.8).

2.1.3 Exchange and Correlation

The difficulty of solving the Schrödinger equation stems from the fact that it is a many-body problem when the system has more than one electron. The reason for this is because the motion of an electron is not independent of other electrons; that is, they are correlated. One aspect of this correlation is accounted for by the Pauli exclusion principle which states that no two electrons of the same spin can occupy the same space at the same time. More generally, this is known as the antisymmetry principle which states that the wave function must change sign when any two electrons are interchanged.

Using a Slater determinant for the wave function satisfies the antisymmetry principle and the exchange energy for like spins is easily accounted for. The difficult part of electron-electron interactions to deal with is the correlation of electrons with opposing spin. This is the central challenge in electronic structure calculations. DFT is one method that is commonly used in calculations that take these interactions into account.

2.1.4 DFT: Hohenberg-Kohn Theorem

The foundation for DFT is based on the Hohenberg-Kohn (HK) theorem [41]. This theorem states that: given a ground-state density $n_0(\vec{r})$ it is

possible to calculate the ground state wave function, $\Psi_0(\{\vec{r}_i\})$. This is a powerful relationship because it also means that all the information that can be known about the system is contained in the ground state density. In other words, the ground state wavefunction is a functional of the density

$$\Psi_0(\{\vec{r}_i\}) = \Psi[n_0(\vec{r})]. \tag{2.9}$$

The original proof of this theorem that was offered by Hohenberg and Kohn [41] started out with the assumption that Ψ_0 was not determined uniquely by n_0 and proceeded to show that this resulted in a contradiction to the variational principle; therefore Ψ_0 must be determined uniquely by n_0.

2.1.5 DFT: Kohn-Sham Equations

DFT looks formally like a single-particle theory (e.g. Hartree-Fock), although the many-body effects are still included via the exchange-correlation functional. This is done by separating the kinetic and potential energy functionals into their single-particle and exchange-correlation components according to [42, 43]

$$E[n] = T[n] + U[n] + V_{xc}[n]. \tag{2.10}$$

The kinetic energy functional $T[n]$ can be decomposed into one part that represents the kinetic energy of non-interacting particles of density n, $T_s[n]$ and one part that represents the remainder $T_c[n]$,

$$T[n] = T_s[n] + T_c[n]. \tag{2.11}$$

The s and c represent single-particle and correlation, respectively. $T_s[n]$ cannot be expressed as a functional of n, but it can be expressed in terms of the single particle orbitals $\phi_i(\vec{r})$ of a non-interacting system with density n, as

$$T_s[n] = -\frac{1}{2}\sum_i \int d^3r \phi_i^*(\vec{r})\nabla^2\phi_i(\vec{r}) \tag{2.12}$$

since for non-interacting particles the total kinetic energy is just the sum of the individual kinetic energies. Because the orbitals are functionals of density, $T_s[n]$ is an explicit orbital functional and an implicit density functional

$$T_s[n] = T_s[\{\phi_i[n]\}]. \tag{2.13}$$

A similar approach is employed for the potential energy functional $U[n]$, which is decomposed as,

$$U[n] = U_H[n] + U_{xc}[n]. \tag{2.14}$$

In this case the full interaction energy is approximated by the Hartree energy, $U_H[n]$, which is the electrostatic interaction energy of the charge distribution $n(\vec{r})$,

$$U_H[n]=\frac{1}{2}\int d^3r\int d^3r'\frac{n(\vec{r})n(\vec{r}')}{|\vec{r}-\vec{r}'|}. \tag{2.15}$$

The difference $U[n]-U_H[n]=U_{xc}[n]$ is included in the exchange-correlation energy functional term. The energy functional Eq. (2.10) can now be written as,

$$E[n]=T_s[\{\phi_i[n]\}]+U_H[n]+E_{xc}[n]+V_{ext}[n] \tag{2.16}$$

where, by definition, $E_{xc}=T_c+U_{xc}$.

Since T_s is written as an orbital functional in Eq. (2.12), it is not possible to directly minimize Eq. (2.16) with respect to n. Instead, a scheme suggested by Kohn and Sham [23] is employed for performing the minimization indirectly. First, Eq. (2.16) is minimized with respect to the density,

$$\begin{aligned}0=\frac{\delta E[n]}{\delta n(\vec{r})}&=\frac{\delta T_s[n]}{\delta n(\vec{r})}+\frac{\delta V_{ext}[n]}{\delta n(\vec{r})}+\frac{\delta U_H[n]}{\delta n(\vec{r})}+\frac{\delta E_{xc}[n]}{\delta n(\vec{r})}\\&=\frac{\delta T_s[n]}{\delta n(\vec{r})}+v(\vec{r})+v_H(\vec{r})+v_{xc}(\vec{r})\end{aligned} \tag{2.17}$$

where $v(\vec{r})$ is the external potential (due to the nuclei) in which the electrons move and $\frac{\delta U_H}{\delta n}$ is the Hartree potential. $\frac{\delta E_{xc}}{\delta n}$ can only be

calculated explicitly once an approximation for E_{xc} has been chosen (see Section 2.1.6). In fact, determining $E_{xc}[n]$ is the central problem in DFT.

Taking a step back and considering a system of non-interacting particles moving in the potential $v_s(\vec{r})$

$$0 = \frac{\delta E_s[n]}{\delta n(\vec{r})} = \frac{\delta T_s[n]}{\delta n(\vec{r})} + \frac{\delta V_s[n]}{\delta n(\vec{r})} = \frac{\delta T_s[n]}{\delta n(\vec{r})} + v_s(\vec{r}), \tag{2.18}$$

the density solving this Euler equation is $n_s(\vec{r})$ [43]. Comparing Eq. (2.18) with Eq. (2.17) it is found that both minimizations have the same solution $n_s(\vec{r}) \equiv n(\vec{r})$ if v_s is chosen to be

$$v_s(\vec{r}) = v(\vec{r}) + v_H(\vec{r}) + v_{xc}(\vec{r}). \tag{2.19}$$

The density of the interacting (many-body) system in potential $v(\vec{r})$, described by a many-body SE in the form of Eq. (2.8), can then be calculated by solving the equations of a non-interacting (single-body) system in potential $v_s(\vec{r})$.

The SE of this auxiliary system

$$\left[-\frac{\nabla^2}{2} + v_s(\vec{r})\right]\phi_i(\vec{r}) = \varepsilon_i \phi_i(\vec{r}) \tag{2.20}$$

yields orbitals that reproduce the density $n(\vec{r})$ of the original system. Note that these are the same ϕ_i's of Eq. (2.12).

The density can then be obtained from the occupation of the orbitals ϕ_i's

$$n(\vec{r}) \equiv n_s(\vec{r}) = \sum_i^n f_i \, |\phi_i(\vec{r})|^2 \tag{2.21}$$

where f_i is the occupation of the i^{th} orbital.

Equations (2.19-2.21) are the Kohn-Sham equations. They effectively reduce the problem of minimizing $E[n]$ to that of solving a non-interacting SE.

2.1.6 Local-Density Approximation

The local-density approximation (LDA) is often used in solutions of the Kohn-Sham equations to approximate the exchange-correlation functional

$$E_{xc}[n] = (T - T_s) + (U - U_H). \tag{2.22}$$

These are small corrections to the Kohn-Sham non-interacting energy and can be calculated accurately for the high and low density limits of a homogeneous electron gas [44] and interpolated as a function of n_0 [45]. One scheme for doing this is by using

$$E_{xc}(n_0) = -n_0 \frac{a_0 + a_1 r_s + a_2 r_s^2 + a_3 r_s^3}{b_1 r_s + b_2 r_s^2 + b_3 r_s^3 + b_4 r_s^4}, \qquad r_s = \left(\frac{3}{4\pi n}\right)^{1/3} \tag{2.23}$$

where a_i and b_j are empirically determined parameters such as the ones used in ref. [45].

Within LDA, the energy of an inhomogeneous electron gas is then calculated using the following local approximation

$$E_{xc}[n(\vec{r})] = \int d\vec{r} n(\vec{r}) \epsilon_{xc}^{n_0}(n(\vec{r}))$$

$$\epsilon_{xc}^{n_0} = \frac{E_{xc}(n_0)}{n_0} \tag{2.24}$$

where the $E_{xc}(n_0)$ is used from (2.23).

This is one simple approximation that is used for obtaining E_{xc}. A more advanced approximation is the Generalized Gradient Approximation (GGA), which is like the LDA but the gradient of the density is also considered in the evaluation of E_{xc} [46]. Yet another more sophisticated treatment of E_{xc} is with the B3LYP hybrid functional that takes on the form

$$E_{xc} = E_{xc}^{LSDA} + a_0(E_x^{exact} - E_x^{LSDA}) + a_x \Delta E_x^{B88} + a_c \Delta E_c^{PW91} \tag{2.25}$$

where a_0, a_x, and a_c are semiempirical coefficients, E_{xc}^{LSDA} is the exchance-correlation energy as determined by the local spin-density approximation (just like LDA but accounts for spin), E_x^{exact} is the exact exchange energy, and E_x^{B88} and E_c^{PW91} are gradient corrections for exchange and correlation, respectively [47].

2.1.7 Basis Sets

In order to obtain numerical solutions to the Kohn-Sham equations, a set of basis functions must be employed to efficiently represent the electronic density/wavefunctions. For finite systems the basis is usually localized in real space. A common approach is to use basis functions that resemble atomic orbitals in order to construct wavefunctions for the system as a linear combination of atomic orbitals (LCAO). The wavefunctions can either be analytic or numerical.

For the analytic approach, Gaussian functions are very popular. The Gaussian function, centered at $\vec{R}_A$, has the form

$$\phi^{GF}(\alpha, \vec{r} - \vec{R}_A) = (2\alpha/\pi)^{3/4} e^{-\alpha|\vec{r}-\vec{R}_A|^2}, \tag{2.26}$$

where α is the Gaussian orbital exponent. Gaussian functions are commonly used because they possess the property that the product of two Gaussians is a third Gaussian. Exploiting this property greatly reduces the time it takes to evaluate two-electron integrals, of which there is a large number in a calculation [40]. Since a Gaussian function is not an adequate representation of an atomic orbital, a contraction (linear combination) of Gaussian functions or "primitives" is used to represent the orbital

$$\phi(\vec{r} - \vec{R}_A) = \sum_{p=1}^{L} d_p \phi_p^{GF}(\alpha_p, \vec{r} - \vec{R}_A), \tag{2.27}$$

where L is the length of the contraction and d_p is a contraction coefficient [40].

In the numerical representation, the orbitals used are similar to atomic orbitals with the exception that a potential is used to eliminate the long range tails of the orbital function [48]. This way the orbital is localized nearby the nucleus. The wavefunction is expanded on a mesh of points in real space. Although some information is lost by discretizing the wavefunction in this manner, reasonable results can be obtained by using a sufficiently fine grid [49]. However, this will always be at the expense of computational speed. The greatest advantage of the grid-based approach is that the molecular orbitals (MO's) that are represented on the grid have a higher flexibility to take on their proper values. The accuracy of the grid-based MO's is only limited by the grid spacing, while the analytic basis function method depends on the number and type of functions in a less straightforward way [50].

For infinite periodic systems, the above procedure is not feasible because an infinite number of atomic orbitals would be required. Instead, a supercell approach is used where only a single repeating cell of the periodic system is considered. Bloch's theorem states that in a periodic

solid each electronic wavefunction can be written as the product of a wavelike part and a cell periodic part f_i [51]:

$$\psi_i(\vec{r}) = \exp[i\vec{k}\cdot\vec{r}]f_i(\vec{r}), \tag{2.28}$$

where $\vec{k}$ is a vector in k-space (the reciprocal space of the periodic lattice) and $\vec{r}$ is a vector in real space. The cell-periodic part of the wave function can be expressed as an expansion of a set of plane waves whose wave vectors are reciprocal lattice vectors of the crystal [52],

$$f_i(\vec{r}) = \sum_{\vec{G}} c_{i,\vec{G}} \exp[i\vec{G}\cdot\vec{r}], \tag{2.29}$$

where $\vec{G}$ is a reciprocal lattice vector defined by $\vec{G}\cdot\vec{l} = 2\pi\cdot m$ with $\vec{l}$ being a lattice vector of the crystal and m is an integer. So, with the use of Bloch's theorem, each wavefunction ψ_i can be represented as a sum of plane waves [52],

$$\psi_i = \sum_{\vec{G}} c_{i,\vec{k}+\vec{G}} \exp[i(\vec{k}+\vec{G})\cdot\vec{r}]. \tag{2.30}$$

The number of plane waves is infinite but an energy cutoff is introduced to reduce their number to a finite value. The sampling is then done at the k-points that are in the Brillouin zone [52]. The accuracy can always be improved by increasing this cutoff energy.

2.1.8 Pseudopotentials

As atoms come together to form a solid or a molecule, the core electrons will only interact weakly with other atoms. It is the valence electrons that strongly participate in bonding. In the pseudopotential (PS) approximation, the properties of a system are determined by the valence electrons while the core electrons do not participate.

The total external potential of the all-electron atom, including the nuclear core and the core electrons, is then replaced by a smooth, non-singular potential (the PS) which acts only on the valence electrons [48]. This greatly reduces the number of electrons for which the K-S equations need to be solved and this is especially significant for metallic atoms lower on the periodic table which have a large number of core-electrons.

2.2 Landauer-Büttiker Theory

This section offers an overview of the Landauer-Büttiker theory [53, 54, 55, 56] for electron transport in mesoscopic systems. The main idea behind this approach is that the current passing through a scatterer from one electrode to another is calculated as a probability that an electron can transmit through the scatterer without being reflected. This approach has

been instrumental in understanding and modeling electron transport through systems at the nanoscale.

A common approach for measuring the conductance of material is by connecting it to two contacts to which a bias is applied thereby inducing a current to pass through the conductor. If the conductor is of macroscopic dimensions with length L and cross sectional area A the conductance is given by

$$G = \frac{\sigma A}{L}, \tag{2.31}$$

where σ is the conductivity of the material. If the length is reduced, the conductance in Eq. (2.31) should increase proportionally. However, experiments have found that the conductance approaches a limiting value (or a multiple of it) $G_0 = \frac{2e^2}{h}$ [57, 58, 59] after the length is smaller than a certain value (the reader is referred to Appendix A for a demonstration of the origin of G_0). Conductors of such dimensions belong to the mesoscopic regime.

An object is considered to be in the mesoscopic regime if L is smaller than the following three characteristic length scales: the de Broglie wavelength λ, which is related to the kinetic energy of the electrons; the (inelastic) mean free path L_m, the distance that an electron travels before its

initial momentum is lost and the phase-relaxation length L_ϕ, the distance that an electron travels before its initial phase is lost [13]. These length scales can vary widely for different materials and they are also dependent on factors such as temperature and magnetic field. For this reason mesoscopic transport phenomena have been observed for dimensions ranging from a few nanometers to hundreds of microns [60].

2.2.1 Reflectionless contacts

An important approximation that is used in the Landauer-Büttiker picture is that the contacts are treated as being reflectionless [13, 54]. This simply means that an electron entering the contact from the conductor will not be reflected back. However, an electron can certainly be reflected as it enters the conductor from a contact and reflection can actually be very large in this case.

In terms of the dispersion relation (Fig. 2.1) this makes for a simplified picture. The $+k$ states (on the positive side of the k-axis) in the conductor are only occupied by the electrons that originated in the left contact, while the $-k$ states (on the negative side of the k-axis) are occupied by those that originated in the right contact. Supposing that both contacts are at the same potential μ_1, the Fermi level for the $+k$ states (as well as the

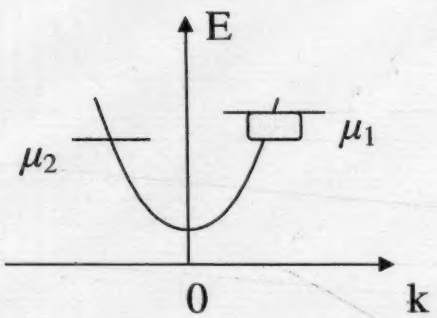

Figure 2.1. Dispersion relation for a single one-dimensional subband. The $+k$ states are on the positive k-axis and filled up to μ_1 while the $-k$ states are on the negative k-axis and filled up to μ_2. In terms of current, the $+k$ and $-k$ states below μ_2 essentially cancel out so that only the $+k$ states between μ_1 and μ_2 need to be considered (blue shaded region).

$-k$ states) is equal to the potential μ_1. However, if the potential at the right contact is changed to $\mu_2 \neq \mu_1$ then it becomes a non-equilibrium situation. It is no longer appropriate to refer to a Fermi level since this term is meaningless in non-equilibrium conditions. Instead, a local quasi-Fermi level is considered which can vary spatially. Since all of the $+k$ states contain electrons originating from the left contact, and only the left contact, which still has its potential at μ_1, then the quasi-Fermi level for the $+k$ states is at μ_1. The same argument can be used to show that the quasi-Fermi level for the $-k$ states is at μ_2.

The above argument about the quasi-Fermi levels of the $+k$ and $-k$ states leads to a convenient simplification: since the current resulting from

the electrons below μ_2 in the $+k$ and $-k$ states essentially cancels out, only the $+k$ states lying between μ_1 and μ_2 need to be considered for calculating the current. In terms of the MO's of the molecule, only those with energies between μ_1 and μ_2 need to be considered in the calculation of current. This is only the case at low temperatures, but this approximation is made to greatly simplify the problem.

2.2.2 Transmission and Reflection

As stated in Section 2.2.1, an electron can be reflected while moving from the contact to the conductor [13, 54]. The probability of this occurring at a given energy is expressed by the reflection coefficient $R(E)$ and the transmission coefficient $T(E)$ is the probability that an electron will transmit through the conductor from one contact to the other, where $T(E)=1-R(E)$. If $T(E)$ is known, the Landauer-Büttiker formula for electron transport is given as,

$$I^{+}=\frac{2e}{h}\int_{\mu_1}^{\mu_2} f^{+}(E)T(E)dE = I^{+}=\frac{2e}{h}\int_{\mu_1}^{\mu_2} T(E)dE \qquad (2.32)$$

where it is assumed that $f^{+}(E)=1$ in this energy range, which is only true at 0 K. The remaining challenge is to calculate $T(E)$ and the next section

outlines a method for doing this involving a non-equilibrium Green's function technique.

2.3 Non-Equilibrium Green's Function

2.3.1 Model of the system

Before proceeding to obtain the transmission probability from the non-equilibrium Green's function, the system being studied needs to be defined. For the model of one molecule bridging two electrodes, the system is divided into three regions as shown in Fig. 2.2. The left lead is semi-infinite: to the left it is repeated infinitely but to the right it connects to the scattering region. The right lead is semi-infinite as well, repeating infinitely to the right but connecting to the scattering region on the left. The molecule of interest is in the scattering region which is finite. Note that the scattering region also includes several layers from each lead, which is necessary for maintaining charge neutrality in this region since there is charge transfer between the molecule and the leads and also to screen the interaction between the molecule and the leads [61].

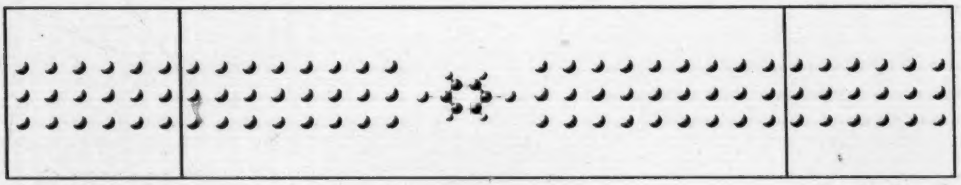

Figure 2.2. The system studied consists of a scattering region containing the molecule of interest as well as several layers of each lead and semi-infinite left and right leads.

2.3.2 Non-Equilibrium Green's Function

The non-equilibrium Green's function (NEGF) formalism is a useful tool in calculating the transmission probability $T(E)$ for an electron passing through a molecule bridging two electrodes. Sometimes referred to as the Keldysh formalism [62], the NEGF allows for the calculation of the infinite system (Fig 2.2) to be performed on only the scattering region, where the effects of the semi-infinite leads are included via self-energies [13, 63], as described below.

The Green's function represents the orbital overlap across the entire system divided by the energy difference between the molecular eigenstates and the Fermi level [64]. Maximizing the coupling elements thereby maximizes the Green's function matrix elements which will, in turn, maximize the conductance. At energy E, the Green's function is given by

$$G(E) = ((E + i\eta)S - H - \Sigma_1 - \Sigma_2)^{-1} \tag{2.33}$$

where H and S are the Hamiltonian and the overlap matrix for the scattering region (including the molecule as well as several layers of each lead) as derived by an *ab initio* method such as DFT (Section 2.1) [13, 63]. η is a small positive infinitesimal whose purpose is to give rise to a finite broadening to the energy levels in the scattering region. During the calculation, its exact value is not significant but it should be on the order of, and slightly larger than the spacings between the energy levels in the leads [63]. Σ_1 and Σ_2 are the self-energies that describe the left and right lead, respectively.

Each self-energy is a complex quantity that accounts for two significant effects experienced by the energy levels in the scattering region as it couples to the leads (Section 2.3.3 outlines the method for determining the self-energies). The real part of the self-energy represents the shift of the energy levels in the scattering region as it couples to the leads and the imaginary part represents the broadening of the energy levels [65]. This broadening can be represented with the broadening matrices Γ_1 and Γ_2 which are defined as the anti-Hermitian parts of Σ_1 and Σ_2

$$\Gamma_{1,2} = i(\Sigma_{1,2} - \Sigma_{1,2}^{+}). \tag{2.34}$$

The spectral function is a useful quantity that can be obtained from Eq. (2.33). It is given by the anti-Hermitian part of the Green's function

$$A(E) = i(G(E) - G^{+}(E)), \tag{2.35}$$

and it leads to the density of states $D(E)$ in the scattering region by taking the trace [63]

$$D(E) = \frac{Tr(AS)}{2\pi}. \tag{2.36}$$

If the Green's function and the broadening matrices, Eqns. (2.33-2.34), are known, the density matrix $[n]$ can be calculated from the relation [63]

$$n = \frac{1}{2\pi}\int_{-\infty}^{\infty}[f(E,\mu_1)G\Gamma_1 G^{+} + f(E,\mu_2)G\Gamma_2 G^{+}] \tag{2.37}$$

where $f(E,\mu)$ is the Fermi-Dirac function describing the population at energy E with respect to a given electrochemical potential μ given by

$$f(E,\mu) = \left(1 - e^{\frac{E-\mu}{k_B T}}\right)^{-1}. \tag{2.38}$$

Equation (2.37) can be used to calculate the self-consistent potential matrix $[U_{SC}]$, which is added to the Hamiltonian of the isolated scattering region (not coupled to the leads) H_0 to yield the Hamiltonian of the scattering region that is coupled to leads

$$H = H_0 + U_{SC}. \tag{2.39}$$

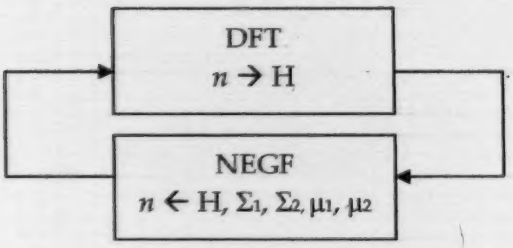

Figure 2.3. Self-consistent cycle between the DFT and NEGF calculations. The density is used to calculate the Hamiltonian in DFT. This Hamiltonian is then used along with the self-energies and the electrochemical potentials in order to calculate the density matrix in NEGF. This density matrix is used in the following DFT calculation and the cycle is repeated until self-consistency is achieved.

Generally, the density matrix $[n]$ from Eq. (2.37) will be different than the one obtained with DFT for the isolated scattering region because, in the Green's function approach, the electrodes will have an effect through the self-energies. For this reason, the density matrix obtained from the Green's function must be used to construct the potential matrix in order to solve the DFT equations. The Hamiltonian obtained from DFT is used to solve the Green's function. This cycle is repeated until self-consistency is achieved between DFT and NEGF (Fig 2.3) [65].

With the above quantities in hand, the transmission function can be calculated as [13, 63, 65]

$$T(E) = Tr(\Gamma_1 G \Gamma_2 G^+). \tag{2.40}$$

This shows that the transmission function is proportional to the broadening due to each lead, given by Eq. (2.34), as well as the Green's function, given by Eq. (2.33), and its adjoint. Equation (2.40) can then be included in the expression for current, Eq. (2.32), to get

$$I = \frac{2e}{h}\int_{\mu_1}^{\mu_2} T(E)dE = \frac{2e}{h}\int_{\mu_1}^{\mu_2} Tr(\Gamma_1 G \Gamma_2 G^+)dE . \qquad (2.41)$$

2.3.3 Determining the self-energy Σ

The self-energies include the presence of the leads in the Green's function so that the infinite problem can be treated with a finite matrix of the same size as the scattering region. The self-energy takes into account the effect that the lead has on the surface atoms (of the scattering region) at the boundary with the electrode. This is accomplished by setting up the Green's function for one of the isolated electrodes as [66]

$$G = \begin{pmatrix} (E+i\eta)S_s - H_s & (E+i\eta)S_{sb} - H_{sb} \\ (E+i\eta)S_{bs} - H_{bs} & (E+i\eta)S_b - H_b \end{pmatrix}^{-1} = \begin{pmatrix} g_s & g_{sb} \\ g_{bs} & g_b \end{pmatrix} \qquad (2.42)$$

where the subscripts s and b are for surface and bulk, respectively. H_s is a finite sized matrix (describing the surface atoms included in the scattering region), while H_b is infinite (describing the rest of the electrode). The goal

is to discover a Σ of the same size as H_s so that the surface Green's function g_s is given by

$$g_s = ((E+i\eta)S_s - H_s - \Sigma)^{-1}. \tag{2.43}$$

In practice, g_s is computed by making use of the periodicity of the infinite contact using techniques described elsewhere [66, 67] (one such technique is described in Appendix B) and Σ is determined by inverting (2.43)

$$\Sigma = (E+i\eta)S_s - H_s - g_s^{-1}. \tag{2.44}$$

This procedure is used to obtain both Σ_1 and Σ_2. Note that the size of the matrices Σ_1 and Σ_2 will generally not be of the same size as the matrices for the scattering region. But this is simply solved by expanding Σ_1 and Σ_2 to the correct size by adding rows and columns of zeros appropriately [66]. It should also be emphasized that since the self-energies for the electrodes are calculated independently, it is possible to perform calculations on systems having two different electrodes.

Chapter 3

Computational methods

This chapter outlines the methods used for obtaining the results described in Chapter 4. The systems studied consist of a BDT molecule bridging two semi infinite metallic leads (composed of Au or Al), as shown in Fig. 2.2. Section 3.1 describes how the geometry optimizations were performed for the system and Section 3.2 outlines how the transport calculations were carried out.

3.1 Geometry optimizations

The geometry optimizations were carried out within the Gaussian program [39]. The model system of the scattering region consisted of a plane of 4 Au atoms constrained to their bulk Au (100) positions to

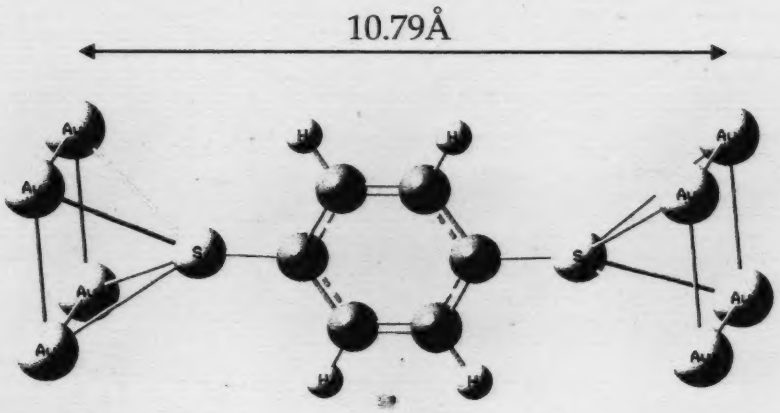

Figure 3.1. The 4Au-BDT-4Au structure used for the geometry optimization. The positions of the Au atoms are held fixed to their bulk positions with the exception that the plane-plane separation was allowed to relax. The entire BDT molecule was allowed to relax.

represent the electrodes next to each S atom in the BDT molecule (Fig 3.1). This model is referred to as the 4Au-BDT-4Au molecule. The geometry of the BDT molecule and the distance between the two Au planes of atoms were allowed to relax. The energy minimum was found for a separation between the two planes of Au atoms of 10.79 Å (electrode-electrode separation). The same approach was employed for the optimizations of the systems with Al electrodes, where the electrode-electrode separation was found to be 9.80 Å. For the BDT molecules containing substituent groups, this distance was held so that the Au/Al atoms were completely

frozen in this position and the substituted BDT molecule was allowed to relax between the electrodes.

The Gaussian calculations were performed on the 4Au-BDT-4Au system using the B3LYP hybrid functional [47, 68] with the 6-31G* basis set for all atoms (including Al) other than gold. This is a split valence shell basis set that also includes polarization functions. Essentially, there are two functions representing each valence orbital. One of these is a contraction of three Gaussians and the other is represented by one Gaussian. The core (non-valence) orbitals are represented by contractions of six Gaussians [40]. For gold atoms, a relativistic effective core potential with a valence basis set [69] was used. This basis set consists of a contraction of 5 Gaussians for the 5s, 5p, and 6s subshells and a contraction of 4 Gaussians for the 5d subshell. Diffuse functions were also added as a single Gaussian for the s-, p- and d-subshells.

Once the optimizations were complete, the electrodes were extended on either side of the 4Au-BDT-4Au structure by adding Au atoms to their bulk positions (FCC with a lattice constant of 4.08 Å) to make the Au-BDT-Au system, as shown in Fig 3.2. Two systems were studied with differing cross sections (3x3 and 5x5). For the Al-BDT-Al

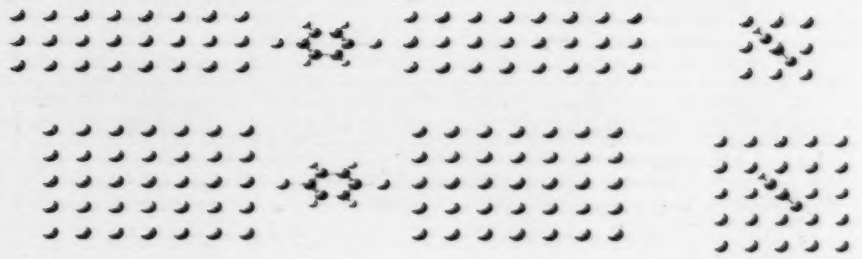

Figure 3.2. The Au-BDT-Au systems used in the calculations. The BDT structure and the electrode-electrode separation were optimized. Au atoms were then added to their bulk crystal positions. The top left and right schematics show the 3x3 Au-BDT-Au system from side and end views, respectively; the bottom left and right schematics show the 5x5 Au-BDT-Au system from side and end views, respectively.

system, the same approach was utilized (also FCC, but with a lattice constant of 4.05Å) to build a system with 3x3 electrodes.

3.2 MATDCAL calculations

The MATDCAL [30] program calculates electron transport in systems like those illustrated in Fig. 3.2 using DFT with LDA (See Section 2.1). The system used consisted of a finite scattering region in between two semi-infinite electrodes, as described in Section 2.3.1 (see Fig. 2.2). Typically, three calculations need to be carried out for a given system: one for each

semi-infinite electrode, from which the self-energies are obtained and one for the finite scattering region which contains the molecule.

Before continuing to the two types of calculations, the basis sets that were used for the MATDCAL calculations are given.

3.2.1 Basis sets

The MATDCAL calculations were performed using norm-conserving pseudopotentials to describe the core electrons [70]. The valence electrons were treated with double zeta polarized (DZP) numerical orbitals for carbon, hydrogen, sulfur, oxygen, nitrogen, fluorine, and aluminum atoms. For the gold atoms, two basis functions were used for the *s* and *d* shells and one was used for the *p* shells. The radial cutoffs were: 5.67 a.u. for carbon, 5.63 a.u. for hydrogen, 5.78 a.u. for sulfur, 4.95 a.u. for oxygen, 5.51 a.u. for nitrogen, 4.51 a.u. for fluorine, 7.10 a.u. for aluminum, and 6.08 a.u. for gold.

3.2.2 Bulk calculations

Bulk systems are composed of a unit cell that is repeated in 3 dimensions as is usual for plane wave calculations of periodic systems (Fig. 3.3). Using a supercell approach, it is also possible to treat wires and isolated

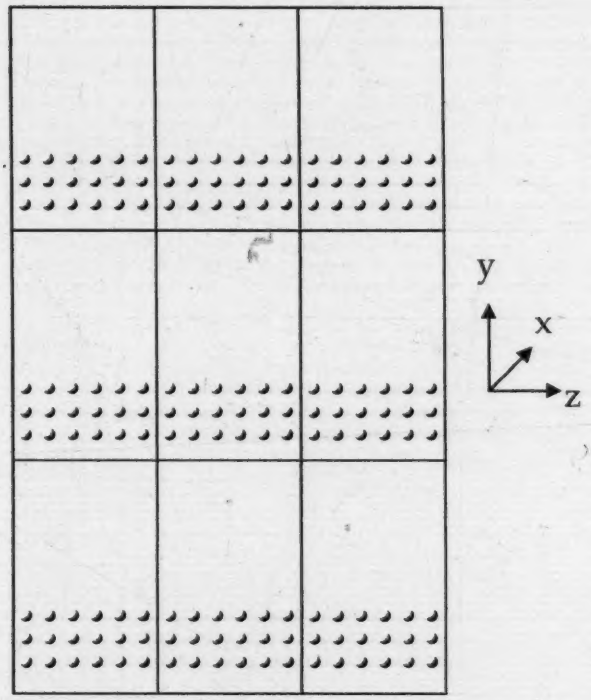

Figure 3.3. A supercell with 8 of its images which show the periodicity. This setup is used to model a nanowire; by including a vacuum region in the x and y-directions there is no interaction between the images in those directions. The cell is repeated infinitely in the x, y and z-directions.

molecules by including a sufficient amount of vacuum space in the unit cell. The unit cell is defined by specifying its dimensions along with the identities and positions of the atoms it contains. For these calculations, the number of grid points on which the basis functions are expanded is also specified along each axis as well as the number of k-points to be used in

reciprocal space. The bulk calculations were used to treat the semi-infinite electrodes in the system.

Table 3.1 contains the values of the parameters that were used for the electrodes of the 3 systems studied. As can be seen from Fig. 3.3 and Table 3.1, the unit cell was bigger in the x and y directions so that the images of the electrode would far enough such that there would be no interaction between the neighbouring unit cells. For the 5x5 Au-BDT-Au system, the cell is much shorter in the z-direction simply because the larger number of atoms greatly increased the computation time. This way the bulk calculation was used to model a nanowire. At least 3 grid points per atomic unit (1 a.u. = 0.529 Å) of length were used for expanding the basis functions along any axis. Notice that only one k-point was needed in the x and y directions since the number of k-points required is inversely proportional to the size of the system. However, 10 k-points were used along the z direction to allow for good treatment of the interactions from image to image in this direction. By systematically increasing the number of k-points in the z direction, it was found that the density of states (DOS) and the bandstructure had converged at this number of k-points for all three systems considered.

Table 3.1. The parameters used for the electrodes in the three systems studied. The dimensions of the cell in the x and y directions are made larger so that images do not interact. At least 3 grid points were used per a. u. along each direction. Only one k-point was needed along the x and y axes since images did not interact in those directions, but 10 k-points were used in the z-direction since interactions in this direction are important to properly model a nanowire.

		system		
parameter	direction	3x3 Au-BDT-Au	5x5 Au-BDT-Au	3x3 Al-BDT-Al
atomic layers	z	6	2	6
cell length (a.u.)	x	40	40	40
	y	40	40	40
	z	23.12	7.71	22.96
number of grid points	x	128	128	128
	y	128	128	128
	z	96	64	96
number of k-points	x	1	1	1
	y	1	1	1
	z	10	10	10

Once the system was defined, the DFT self-consistent calculation was carried out for each electrode. The results were used to obtain the DOS, bandstructure, eigenstates, and the charge on each atom with a population analysis. The result from the self-consistent calculation were also be used to calculate the self-energy for each electrode in the two-probe calculation of the entire system.

3.2.3 Two-probe systems

The calculation for a two-probe system is more complicated than for a bulk system because it consists of two semi-infinite electrodes and a finite scattering region. However, the system is divided into three parts which can be dealt with individually. As mentioned above, a bulk calculation is carried out for each electrode. The results from these are used to obtain the self-energies that represent the influence on the scattering region coming from each electrode, as described in Section 2.3.3.

The scattering region is similar to a bulk system with the main difference being that it is not periodic in the z-direction, which is the direction in which the electrodes are semi-infinite (and also the direction of electron transport). A two probe system is shown in Fig. 3.4 with two of its images in the y direction. It should be emphasized that the left and right electrodes are shown for clarity but they are actually included in the calculation as self-energies.

Because the system represents semi-infinite electrodes connected to a finite scattering region, some atomic layers from each electrode need to be included in the scattering region. These layers are included so that they can screen off the effects that the molecule and the electrodes have on each other and are referred to as screening (or buffering) layers. One such effect

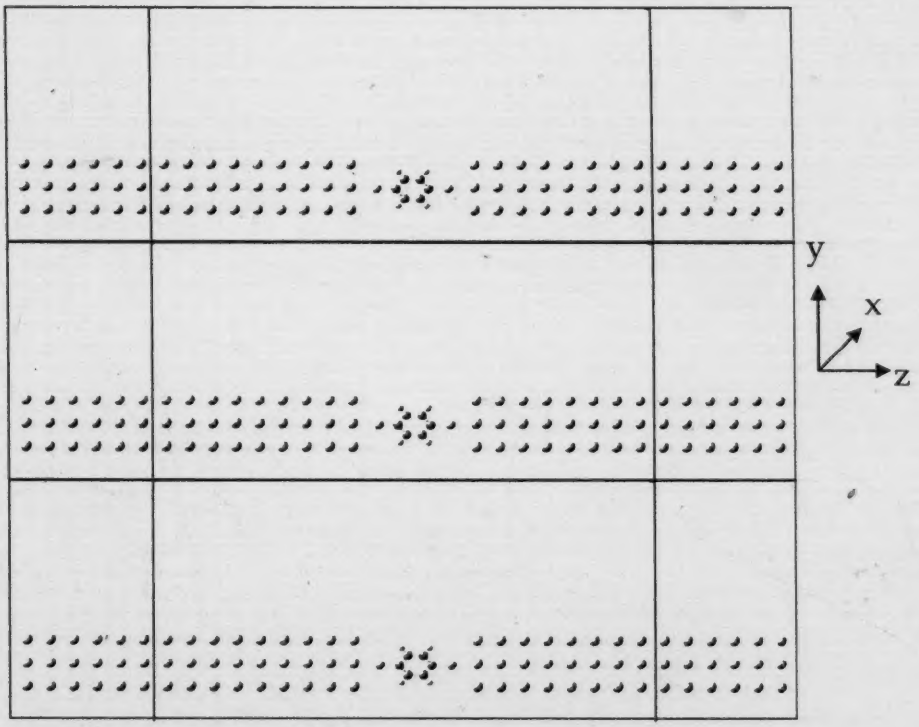

Figure 3.4. A two-probe system and two of its images in the y-direction consisting of a scattering region between left and right electrodes. The electrodes are semi-infinite and the entire structure is repeated in the x and y-directions.

is charge transfer: as a molecule binds to an electrode, its energy levels will broaden and there can be a transfer of charge from one to the other due to the electronegativity differences between the atoms that are involved in the binding [37, 71, 72]. The inclusion of screening layers ensures that charge neutrality is preserved in the scattering region. The screening layers also ensure that there is a close match between other

quantities such as the potential and electronic density at the interfaces between the scattering region and the semi-infinite electrodes [18].

The accuracy of the calculation increases asymptotically with the number of screening layers but this is at the expense of computation time. It was found that, for the 3x3 Au-BDT-Au and 3x3 Al-BDT-Al systems, charge neutrality was sufficiently maintained (deviation from neutral was less than 0.08 electrons in the worst cases) when 9 and 8 screening layers were used between the molecule and the left and right electrodes, respectively (see Fig. 3.4). The reason for a different number of layers on each side is because of the nature of the Au (and Al) electrodes in the (100) direction which consist of two alternating atomic layers. The 5x5 Au-BDT-Au system maintained the same degree of charge neutrality with only 3 and 4 screening layers between the molecule and the left and right electrodes, respectively. The reason why so comparatively few layers were needed for the 5x5 electrodes is because the screening is more effective with larger cross sections.

Table 3.2 contains the values of the parameters that were used for the scattering regions of the three systems studied. As for the bulk systems representing the electrodes, the cell is made large enough along the x and y axes so that there would be no interaction between

Table 3.2. The parameters used for the scattering region in the three systems studied. The dimensions of the cell in the x and y directions are made larger so that images are too far apart to interact in these directions. At least 3 grid points were used per a. u. along each direction. Only one k-point was needed in the x and y-directions since images did not interact in those directions and there was no value for k-points in the z-direction since the scattering region is not periodic in this direction.

		system		
parameter	direction	3x3 Au-BDT-Au	5x5 Au-BDT-Au	3x3 Al-BDT-Al
screening layers (left / right)		9 / 8	3 / 4	9 / 8
cell length (a.u.)	x	40	40	40
	y	40	40	40
	z	82.04	43.51	79.74
number of grid points	x	128	128	128
	y	128	128	128
	z	256	160	256
number of k-points	x	1	1	1
	y	1	1	1

neighbouring unit cells. In fact, these dimensions need to be the same for the scattering region as they were for the electrodes. Once again, at least 3 grid points were used per a.u. of length along each axis to numerically represent the basis functions. Since there is no periodicity along the z-axis for the scattering region, no value for k-points along this direction is needed.

As mentioned above, the self-consistent calculation begins by determining the self-energies using the results of the bulk calculations performed on each electrode. The self-energies are then used in the NEGF part of the DFT/NEGF self-consistent procedure (see Fig. 2.3). After convergence, the DOS, scattering states, transmission spectra, and charges can be calculated. The application of a bias to each electrode can also be simulated. Fortunately, the self-energy calculations do not need to be repeated at different biases. The zero bias calculation serves as a reference and the energy levels along with the electrochemical potential are shifted appropriately in energy during the calculation for the self-energy. Therefore the bias is included directly into the self-energy. The current at each bias is calculated by integrating under the transmission function in the range between the electrochemical potentials of the two electrodes (see Eq. (2.41) in Section 2.3.2) and current-voltage plots can be obtained.

Chapter 4

Results and Discussion

4.1 The Au-BDT-Au system

The Au-BDT-Au system has received much attention in both theoretical [35, 36, 37, 38, 73, 74, 75] and experimental [8, 76, 77] electron transport studies. The BDT molecule is a good candidate for such studies because of its relatively simple structure and since the thiol groups bind readily to gold surfaces because it has the possibility to form multiple bonds with the surface metal atoms [78]. BDT also has a conjugated π ring that offers delocalized electronic states which are beneficial to electron transport because they can form a scattering state through which an electron can transmit from one electrode to the other [38].

As BDT binds to a gold electrode, the thiol (-SH) group loses an H atom and the S atom forms strong covalent bonds to the gold surface [78],

$$RS\text{-}H + Au_n^0 \rightarrow RS^- Au^+ \cdot Au_{n-1}^0 + \tfrac{1}{2}H_2 . \quad (4.1)$$

It is not completely understood what happens to the $\frac{1}{2}H_2$ in this reaction but it is believed that it ends up as a $H_{2(g)}$ molecule [79]. Because there are two thiol groups on opposite ends of the BDT molecule, it can form a molecular bridge between two Au surfaces, thus forming the Au-BDT-Au system. These surfaces can act as electrodes that can be biased in order to run an electric current through the BDT molecule.

There has been a great effort to understand the binding of BDT on various Au surfaces, e.g. (100), (110), (111) [35, 36, 37, 38], because it has been found that even small variations in binding geometries can lead to significant differences in conductance [36, 37, 38]. For example, one study [37] showed that there was a difference in conductance of about a factor of 5 between BDT bridging two Au (100) and (111) surfaces, where the (100) surface yielded the higher value. The same study also found that if the S atom in the BDT molecule is connected to the surface through a single Au atom that is itself on top of the Au surface, this would also affect the conductance dramatically, increasing it by over one order of magnitude. Another theoretical study [38] has shown that small variations in the Au-S

bond distance could change the conductance significantly. This high sensitivity of conductance to geometry is one of the explanations given for the lack of agreement between different results, both experimental and theoretical, where there is still a discrepancy between the two by a factor of ca. 50 for the BDT molecule [32].

The present work concentrated on binding to the Au (100) surface on which the thiol group can bind favourably in several ways including binding to the hollow site, bridge site, and top site as shown in Fig. 4.1. Hollow site binding was investigated because it is the most energetically favourable of the three (binding energies: 3.41 eV for hollow site, 2.50 eV for bridge site, and 1.60 eV for top site [35]), and previous calculations on this system are also available in the literature [35, 37], to which the results from this work can be compared. In the case of hollow site binding of BDT to an Au (100) surface, the sulfur atom binds to four Au atoms. The geometry optimization was performed on the 4Au-BDT-4Au system and the 3x3 Au-BDT-Au system was then built around this structure as described in Section 3.1.

As a molecule binds to metallic electrodes, its discrete energy levels get broadened due to their coupling to the continuous levels of the electrode [63]. This contributes to the nature of the DOS, but it is difficult

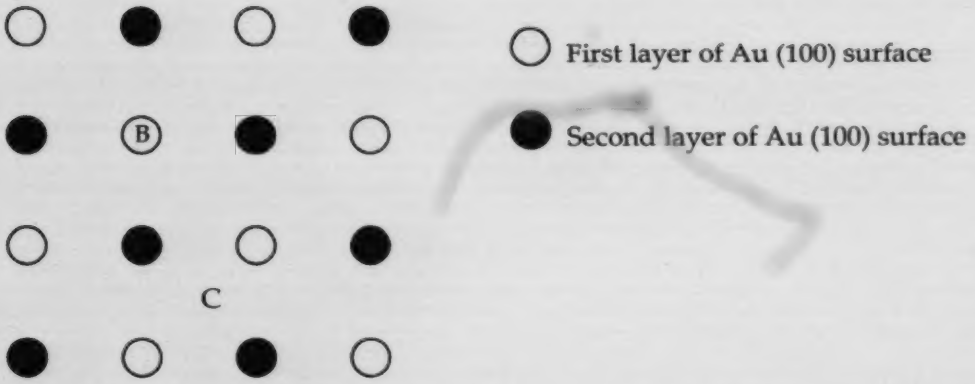

Figure 4.1. The atomic arrangement of the first two layers of an Au (100) surface along with the positions of the hollow site (A), top site (B) and bridge site (C) where a S atom can bind.

to discern the broadened molecular levels from the DOS of the electrodes since there are more of the latter and they tend to overwhelm the spectrum (see Fig. 4.2). Fortunately there are some circumstances under which the broadening of a single molecular level can be directly observed in the DOS, as is discussed in Sections 4.3 and 4.5. In those cases the DOS of systems with and without the molecular orbital (MO) are compared and the difference clearly stands out. One such broadened state is referred to as a scattering state which can be thought of as an eigenstate for the open system (the molecule bridging two semi-infinite electrodes). If the scattering state is coupled to both electrodes, it will provide a conduit through which an electron can pass from one electrode to the other. This

type of scattering state leads to one mode of transport through the system and the transmission spectrum is a sum of the contributions coming from all of the scattering states. Note that not all of the scattering states allow for transmission, some result in reflection (see Fig. 4.8 for an example).

4.2 Transport through the 3x3 Au-BDT-Au system

The transmission function represents the probability that an electron with a given energy will transmit through a molecule from one electrode to the other. As described in Section 2.3.2, the integral of the transmission gives the current for a particular bias window. Figure 4.2 shows the transmission function and the DOS for the 3x3 Au-BDT-Au system. The positions of some of the σ-type (o) and π-type (x) MO's of the 4Au-BDT-4Au system are also included for comparison. The energy axis of both plots is relative to the Fermi level of the electrodes which is at -3.84 eV, while the experimental value for bulk Au is -5.1 eV. The large discrepancy between the two is likely due to the fact that nanowires of finite cross section were modeled in this work as opposed to bulk Au.

As mentioned in Section 4.1, it is not trivial to relate the DOS to molecular eigenstates. In Fig. 4.2, there are two sharp peaks in the DOS at -0.38 and 0.48 eV that are near MO's. It is later revealed (see the discussion

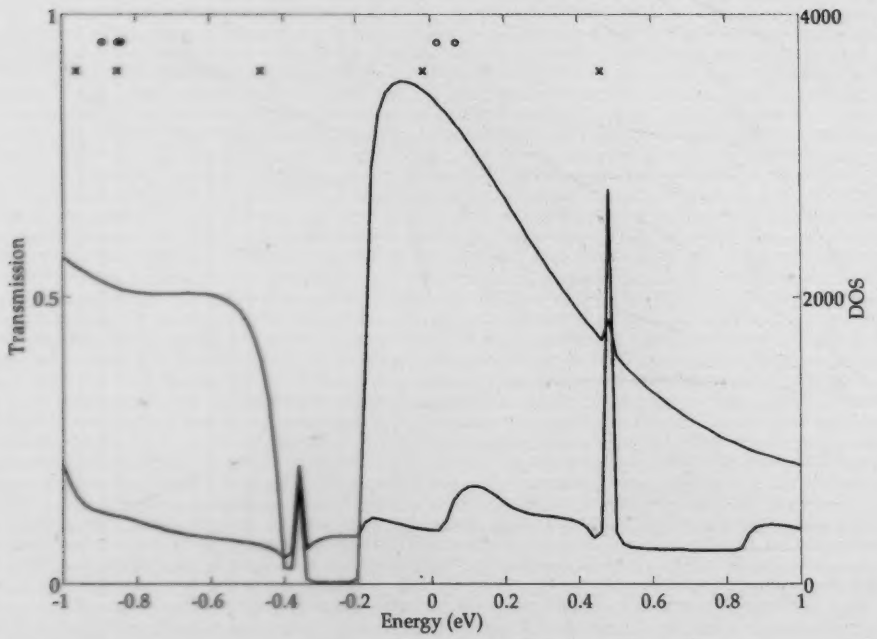

Figure 4.2. Transmission spectrum and DOS for the 3x3 Au-BDT-Au system at zero bias. The position of the eigenstates from the 4Au-BDT-4Au molecule are shown at the top: (o) for σ-type MO's and (x) for π-type MO's. The energy scale is relative to the Fermi level of the electrodes (-3.84 eV).

on Fig. 4.6 in Section 4.3) that only the peak at -0.38 eV is due to a MO, while the peak at 0.48 eV is due to states originating in the electrodes.

It is not possible to predict the nature of the transmission spectrum based solely on the DOS spectrum. The only definitive connection between the two is that there will be no transmission where there is no DOS because states have to be present for an electron to transmit.

However, just because there are states in an energy range, it does not guarantee that there will be transmission, a suitable MO must also be nearby. An example of this can be seen around -0.3 eV in Fig. 4.2 where the DOS shows that there are states but the transmission is essentially zero. The states must couple to both electrodes so that they spatially extend from one electrode to the other in order to contribute to transmission (this can be seen from the scattering state at that energy, vide infra). An interesting feature of the transmission spectrum shown in Fig. 4.2 is that it is fairly smooth with the exception of two sharp features located at -0.36 and 0.48 eV. These are artifacts in the calculated transmission at those values that are due to the intense sharp peaks in the DOS. For the purposes of these calculations, they will not play a significant role since they are too small to contribute a noticeable amount to the current of the system that is determined by integration of the transmission.

Comparing the MO's to transmission is more intuitive. This is because there is always a MO associated with every transmission peak. As will be discussed in Section 4.3, it is the π-type MO's that contribute the most to transmission. With this knowledge, it is fairly straightforward to assign the π-type MO's to features in the transmission spectrum: the MO

at -0.02 eV leads to the large peak near the Fermi level, the MO at -0.42 eV leads to the shoulder near that energy and this continues to the left towards the two MO's at -0.85 and -0.95 eV. The broadening of the MO's becomes apparent by looking at the width of the transmission peaks, and because the transmission is continuous in between MO's, as in the range [-0.85,-0.48] eV. It is interesting to note that the transmission coefficient (height of the transmission) near the Fermi level is close to unity, while to the left of -0.4 eV it is close to one half. This shows that different MO's can contribute different amounts to the transmission.

Figure 4.3 shows the DOS and transmission spectra for the 3x3 Au-BDT-Au system at different biases that are applied to the right electrode. The application of a bias to an electrode essentially shifts its energy levels as well as the electrostatic potential μ by $-qV$ where q is the charge of an electron and V is the bias. With the DOS (Fig 4.3, top), it is apparent that many of the features are shifted to the left with increasing bias. The sharp peak at -0.36 eV seems to broaden as it moves to the left. It is interesting to note that the very high and sharp peak at 0.48 eV seems to get split into two peaks for finite biases. The second peak that appears is located at about $-qV$ in energy from the position of the original peak. This is an indication that this sharp peak is due to DOS that are localized in the

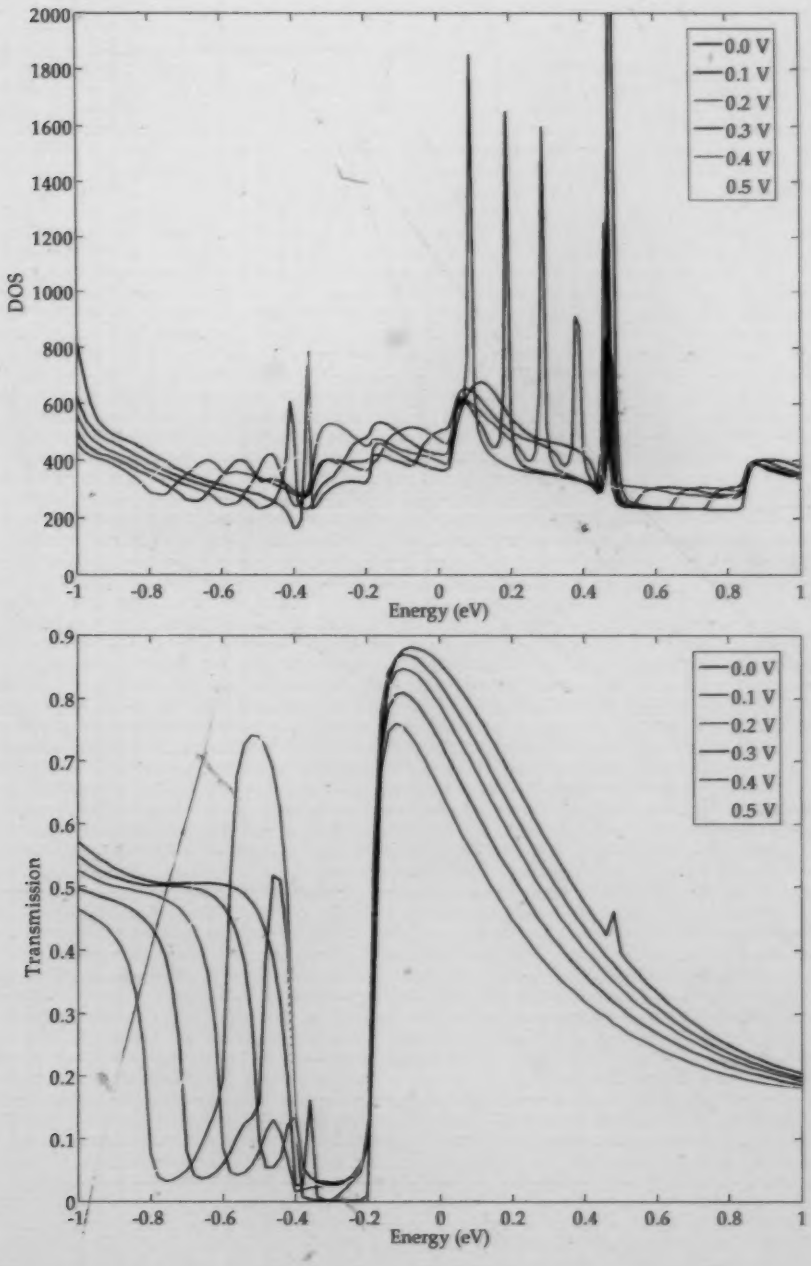

Figure 4.3. DOS (top) and transmission spectra (bottom) for the 3x3 Au-BDT-Au system for different biases applied to the right electrode. The energy is relative to the Fermi level of the left electrode which was at -3.84 eV.

electrodes since levels in the molecule would only shift by ca. $-qV/2$, as described below.

The entire transmission spectrum (Fig. 4.3, bottom) essentially gets shifted to the left as the bias on the right electrode is increased. The energy levels and μ of the left electrode remain unchanged but the energy levels and μ of the right electrode are shifted by $-qV$. This means that the entire voltage drop occurs in the molecule [80] and its energy levels shift by approximately $-qV/2$. It can be seen that the transmission spectrum is shifted to the left by ~0.05 eV for each additional 0.1 V of bias applied to the right electrode. Of course this is only the most obvious change in transmission with respect to bias. Additionally, as the energy levels in the molecule move with respect to the states in the electrodes, the coupling between the molecule and the electrodes may improve or worsen and this will have a more subtle effect on transmission.

One part of the transmission spectrum remains essentially the same at all biases. The region of [-0.4, -0.2] eV has low transmission at any bias. This results in an interesting effect as described below. Note how the high transmission peak is shifted to the left into this region but reappears on the left side at higher biases, e.g. at -0.6 eV for the 0.5 V plot. This indicates

that, for reasons explained below, the transmission is suppressed in the [-0.4, -0.2] eV region.

Since the current can be calculated by integrating under the transmission curve in the range between the electrochemical potentials of the left and right electrodes, it directly follows that at low bias the current is related to the transmission near the Fermi energy since this is where the integration would be carried out. Taking the value of the transmission at the Fermi level from Fig. 4.3 at zero bias gives a low bias conductance of 66 μS for this system. For comparison, the quantum of conductance is G_0 = 77.5 μS, so this is a good indication that the BDT molecule in this system conducts well at low bias. Experimental measurements on the Au-BDT-Au system have shown conductance on the order of 0.8 μS [76], which is about two orders of magnitude lower than the value obtained in this work. Unfortunately, this kind of disagreement between theory and experiment for this system is common with most calculations yielding conductance that is one to two orders of magnitude higher than experiment [32]. As mentioned in Chapter 1, there are many possible sources for the disagreement between theory and experiment. In most experiments the binding arrangement of the molecule to the electrodes is not known, and neither is the structure of the electrodes. Since there is

such a high sensitivity of the conductance to binding geometry, this can account for this discrepancy. Of course, the computational model also has its limitations such as the use of 3x3 nanowires as opposed to bulk electrodes, the assumption that the 4Au-BDT-4Au optimized structure would be adequate for this model, and that densities obtained using LDA are sufficiently accurate.

The current-voltage (I-V) curve for the appropriate integrations under the curves in Fig. 4.3 is shown in Fig. 4.4. An interesting feature of this plot is that, although the current mostly increases with higher bias, there is a region between 0.2 and 0.4 V where the current actually decreases as the bias increases. This kind of behaviour is referred to as negative differential resistance (NDR), which can be an attractive characteristic for molecular electronics. It is the defining behaviour in resonant tunneling diodes (RTD) [81, 82], which are two-terminal devices that offer great utility in switching and in performing logic operations. RTD's offer an advantage over conventional devices because they should be easier to integrate than three-terminal devices and can also outperform them. However, the NDR predicted here is not significant enough to be of any real use in an actual molecular device.

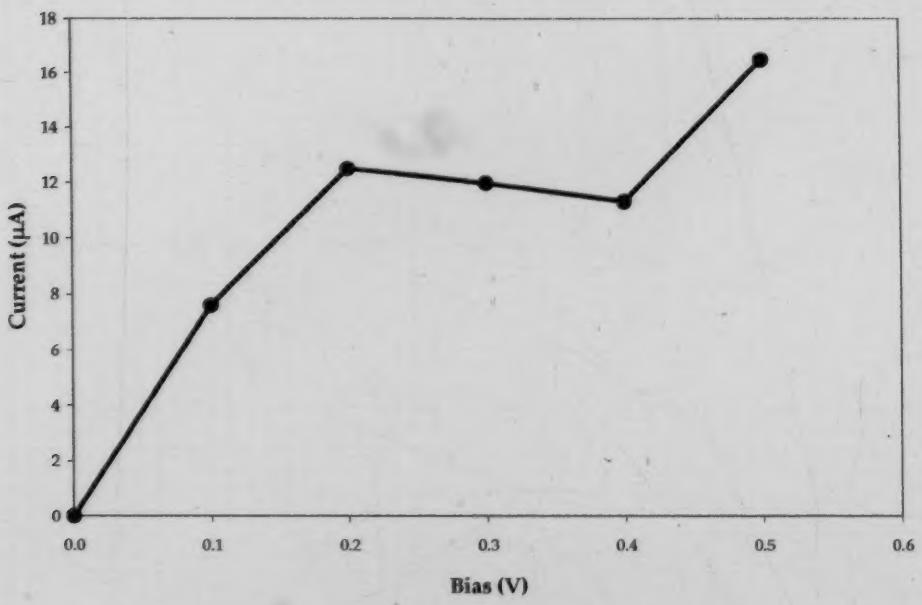

Figure 4.4. I-V plot for the 3x3 Au-BDT-Au system shown in Fig 3.2.

The NDR can be explained by considering the region between -0.4 and -0.2 eV of the transmission spectra (Fig. 4.3, bottom) where the transmission is nearly zero for all biases. This means that this region will not contribute to the current. At the same time, the high transmission peak near the Fermi level is shifted to the left and its presence in the [-0.2, 0.0] eV range decreases. Therefore, for biases between 0.2 and 0.4 V, the region of low transmission gets included in the integration while the transmission peak is diminishing. This results in a lowering of current even though the bias is increased. The NDR that is exhibited in this system

is entirely due to the nature of the electrodes that have a finite cross section and do not behave as truly "metallic" leads (vide infra). More specifically, they do not have a continuous distribution of states that can couple in a manner that is beneficial to transport in the [-0.4, -0.2] eV range. Note that the NDR is not due to deficiencies in the computation method. This phenomenon has also been observed by others [37] in calculations on a similar system with the same 3x3 electrodes. In that work, the NDR occurs in the region between 0.2 V and lasted until 0.6 V. It is interesting to note that this feature can be seen for each of the two electrodes for higher biases since the energy levels of the right electrode are shifted with respect to those of the left electrode, e.g. the spectrum for 0.5 V in Fig. 4.3 has two regions of low transmission: one between -0.4 and -0.2 eV due to the left electrode, and the other between -0.9 and -0.7 eV due to the right electrode which is shifted by -0.5 eV. The NDR effect is not present if electrodes with higher cross sections are used (Section 4.4) but the calculations are more costly. For the purposes of this work, the lower cross section electrodes are used in order to study effects that do not depend on this NDR feature, while keeping in mind that it is indeed an artifact of the electrodes and not a characteristic of the BDT molecule.

4.3 The effect of substituent groups on transport through the 3x3 Au-BDT-Au system

Different substituent groups were added to the BDT molecule at the 2- and 5- positions (Fig. 4.5) in order to determine how changes in the electronic properties of the molecular system affect the conductance of the molecule. The substituents used span a range from electron donating groups (EDG) to electron withdrawing groups (EWG). The goal was to determine how substituent groups could be used to effectively tune the conductance of the BDT molecule. With this ability it would then be possible to design a molecule with desired electronic properties.

The geometry optimizations were carried out as described in Section 3.1. The DOS and transmission spectra were calculated for the 11 systems containing different substituent groups. Figure 4.6 shows a sample of the DOS and transmission spectra at zero bias for three systems including the EDG NH_2 and EWG NO_2 groups as well as the unsubstituted BDT molecule (R=H).

The DOS for the three systems are quite similar with just a few different features. One difference that stands out is the position of the sharp peaks at -0.25 and -0.38 eV for the molecules with the NH_2 and H substituents, respectively. These peaks seem to be spaced by about the

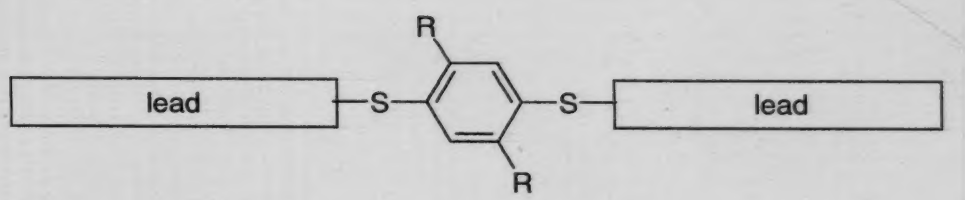

$R = N(CH_3)_2$, NH_2, OH, OCH_3, CH_3, H, COOH, CHO, CF_3, CN, NO_2

Increasing ED

Increasing EW

Figure 4.5. Substituted BDT system used. The substituent groups span a range from the electron donating $N(CH_3)_2$ to the electron withdrawing NO_2. For each system the two R groups would be the same.

same amount as the MO's for those systems at -0.35 and -0.45 eV, so this is a good indication that these peaks are due to molecular states. There is no such peak for the system containing the NO_2 substituent although this system has a higher shoulder on the DOS at -0.5 eV. It can therefore be concluded that these features on the DOS are due to the molecular orbitals since they differ for each system. On the other hand, the sharp intense peak at 0.48 eV is present for all systems, at the same energy even though the MO's near it differ in energy. This is further evidence that this peak comes from states in the electrodes.

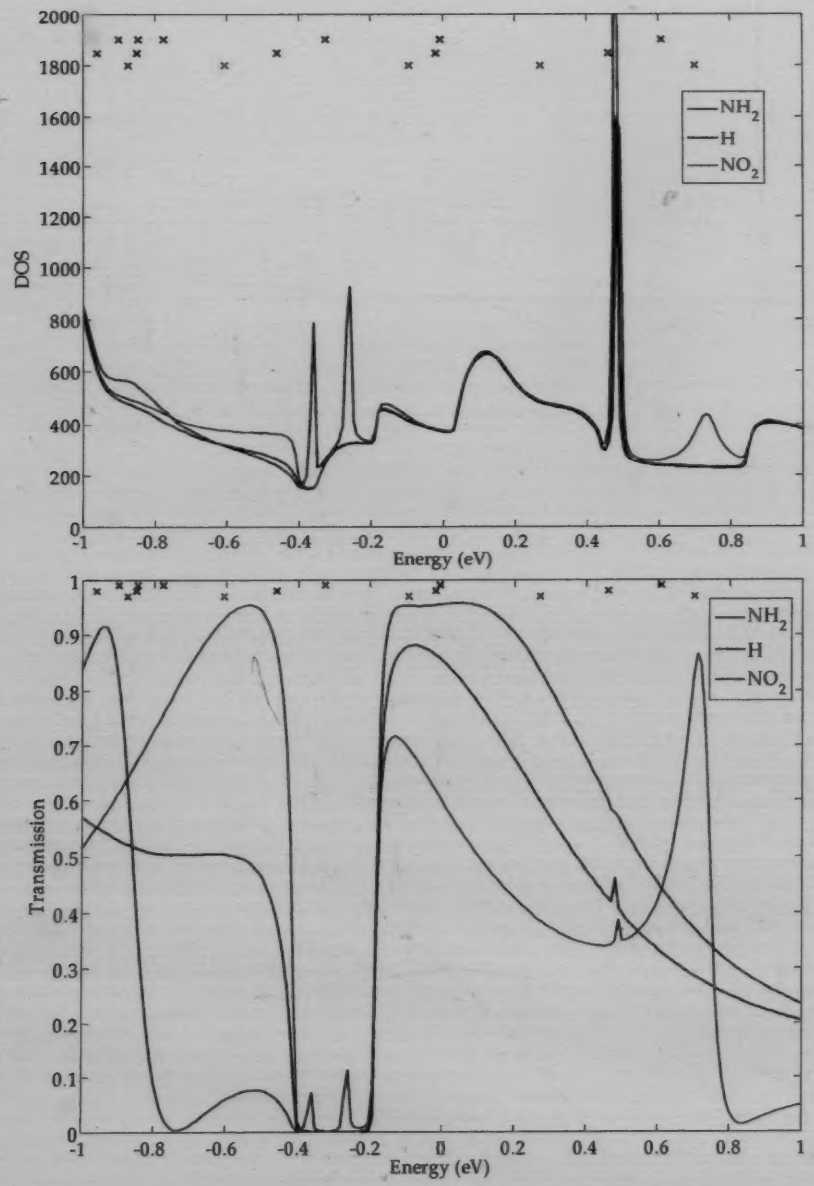

Figure 4.6. DOS (top) and transmission spectra (bottom) relative to the Fermi level of the electrodes (-3.84 eV) for three different substituents at zero bias including the EDG NH_2 and EWG NO_2. The positions of the π-type MO's of the 4Au-BDT-4Au molecule are shown at the top for each system.

A nice demonstration of how a molecular level gets broadened can be seen in the DOS peak near 0.7 eV for the system containing NO_2. Since this peak is absent for the other two systems, which can be thought of as control cases, this is evidence that this is indeed a broadened molecular state. There is a MO close to this energy for the NH_2 substituted system that does not display this broadening. This is shows that not every π-type orbital will couple well with the states from the electrodes and broaden by doing so.

For the purposes of this work, the most important feature of the transmission spectrum is the value at and near the Fermi level (0 eV). The trend that is shown in Fig. 4.6 held for all 11 substituents, namely that BDT substituted with EDG's have a higher transmission near the Fermi level than unsubstituted BDT; while BDT substituted with EWG's have a lower transmission near the Fermi level than unsubstituted BDT. This can be explained by the positions of the highest occupied molecular orbitals (HOMO) for each system. The HOMO of the system containing NH_2 is the closest to the Fermi level, thus it has the highest transmission at the Fermi level, and the HOMO of the system containing NO_2 is the farthest from the Fermi level so it has the lowest transmission at the Fermi level. The sharp peaks at 0.48 eV in the DOS have a small effect on the smoothness of

the transmission at this energy. Once again, this feature is a result that comes out of the intense peak in the spectra. There is a high transmission peak near 0.7 eV for the NO_2 substituted system which is not present for the other two systems. It likely corresponds to the broadened DOS peak for this system at the same energy that was mentioned above.

Another point to consider about the transmission spectra in Fig. 4.6 is that, as for the unsubstituted BDT case (Section 4.2), there is a low transmission range from -0.4 to -0.2 eV that will lead to NDR. Since this is consistent for all 11 substituents, it gives further evidence that the NDR effect is due to the nature of the electrodes and not the BDT molecule. The three substituted systems have π-states near the left side of this window of low transmission. The NO_2 substituted system has a level just outside the window, near -0.6 eV that results in a high transmission peak. The H and NH_2 substituted systems have their levels inside the window and this only results in two small sharp peaks inside the [-0.4, -0.2] eV region. So it seems that in this window the transmission is suppressed by the lack of states in the electrodes for the molecule to couple with. However the effect from these MO's can also be seen in the transmission outside of the [-0.4, -0.2] eV region, near -0.5 eV, where the H substituted system has a

moderate transmission and the NH_2 substituted system has a lower transmission since its level is farther away.

Since the low transmission window was present on the spectra for all substituents, it will not affect the relative conductance values of the substituted BDT molecules. The main consequence is that the I-V curves for all systems would show NDR behaviour just like in the unsubstituted 3x3 Au-BDT-Au system.

A scattering state of an open (two-electrode) system is analogous to an eigenstate in a molecule. In the same way that an eigenstate describes an electron in an isolated molecule, a scattering state describes an electron passing through the molecule from one electrode to the other (or reflecting back to the electrode it originated from). By looking at the scattering state it is possible to determine to which orbital of the molecule it corresponds, if any. The scattering state corresponding to the peak of the transmission spectrum near the Fermi level for R=H in Fig. 4.6 is shown in Fig. 4.7. A visual comparison shows that it corresponds to the HOMO of the isolated molecule. This comparison was made for all substituted BDT systems and it was confirmed that the transmission near the Fermi level is mostly through the HOMO of the molecule. This agrees with the positioning of the MO's in Fig. 4.6. It also agrees with a previous theoretical study on a

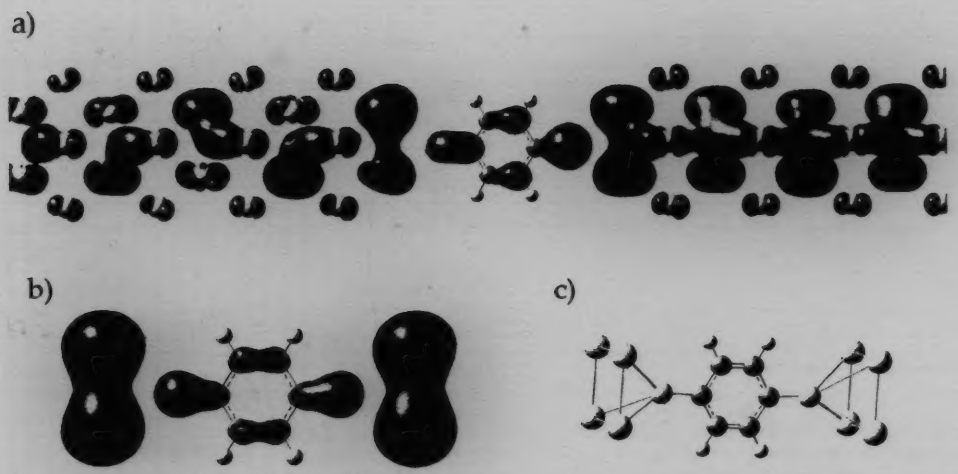

Figure 4.7. a) The scattering state for the unsubstituted (R=H) 3x3 Au-BDT-Au system in Fig. 4.6 at the peak of the transmission curve (-0.08 eV). b) The HOMO of the 4Au-BDT-4Au system shown in c). Note the resemblance between the scattering state and the HOMO which confirms that transmission peak is due to conductance through the HOMO level. The colours represent the phase.

similar system with a series of substituents [75], which also concluded that the HOMO plays the most significant role in transmission at low bias because of its proximity to the Fermi level and its delocalized nature.

Figure 4.8 shows an example of a reflection scattering state. It originates from -0.3 eV in the transmission spectrum for the H substituted Au-BDT-Au system in Fig. 4.6. Note how there is no amplitude on either the molecule or on the right electrode.

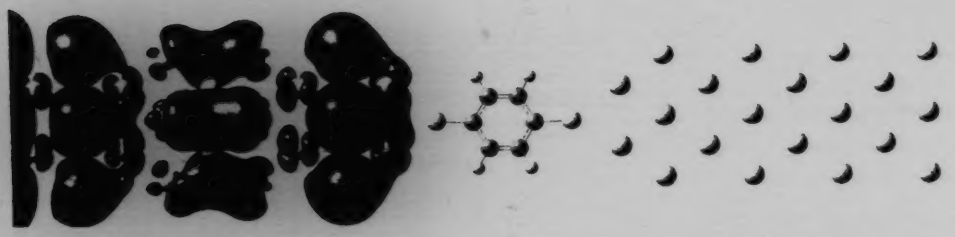

Figure 4.8. A scattering state showing reflection for the unsubstituted (R=H) 3x3 Au-BDT-Au system in Fig. 4.6 at -0.3 eV, where the transmission is close to zero.

Generally, it is the delocalized π-type MO's that are beneficial to transmission and highly localized σ-type MO's play a much smaller role [38, 75, 83]. This is because π-type MO's can form scattering states that are delocalized from one electrode, through the molecule, to the other electrode thus providing a conduit through which an electron can transmit. For the unoccupied MO's, the lowest unoccupied molecular orbital (LUMO) and LUMO+1 were found, for all substituents, to be σ-type MO's and the closest delocalized unoccupied MO to the Fermi level was LUMO+2 which is relatively far from the Fermi level compared to the HOMO (Figs. 4.2 and 4.9). This result is in agreement with the previous theoretical study on a similar system with several substituents [75] that also found the LUMO and LUMO+1 to be localized and have a negligible contribution to transmission.

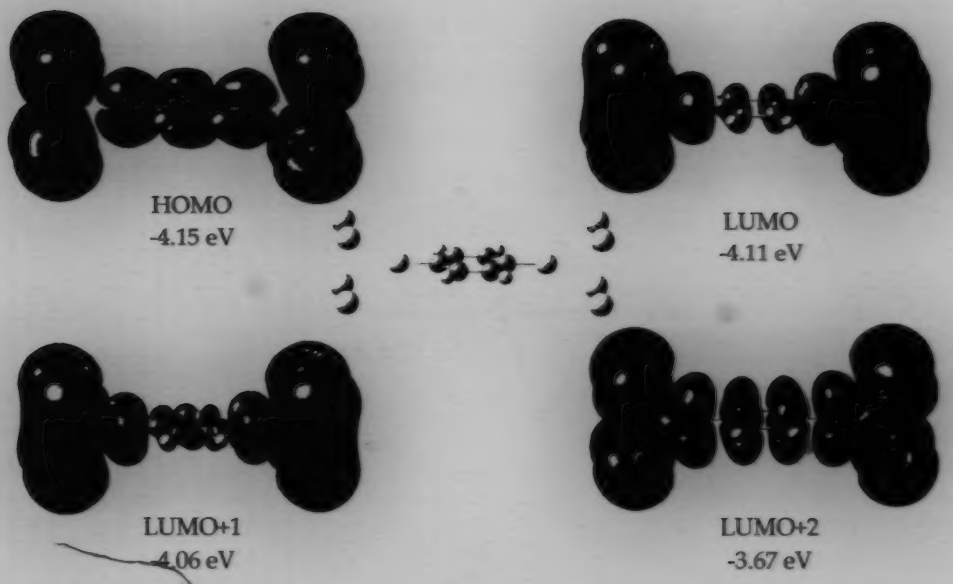

Figure 4.9. Molecular orbitals of unsubstituted 4Au-BDT-4Au that are close to the Fermi level in the Au-BDT-Au system. The HOMO and LUMO+2 are π-type orbitals with a nodal plane along the benzene ring. The LUMO and LUMO+1 MO's are σ-type orbitals.

Substituent groups have an effect on the position of the energy levels in a molecule. In BDT, EDG's raise the energy of the HOMO level while EWG's lower it (Table 4.1). This phenomenon was explained in a theoretical study of ionization potentials for disubstituted benzenes [84] as follows: when an EDG binds to a benzene molecule, two filled MO's combine, thus forming a stabilized and a destabilized MO. The destabilized MO is the HOMO of the substituted benzene, which is higher

Table 4.1. Position of the HOMO and LUMO+2 levels for the 11 substituted 4Au-BDT-4Au systems. The Hammett substituent constant σ_p [85] which is a measure of the strength of a group as an EDG/EWG is also included. The EDG's are at the top of the table and the EWG's are at the bottom.

substituent	σ_p	HOMO energy (eV)	LUMO+2 energy (eV)
$N(CH_3)_2$	-0.83	-4.03	-3.50
NH_2	-0.66	-4.07	-3.46
OH	-0.37	-4.28	-3.70
OCH_3	-0.27	-4.03	-3.49
CH_3	-0.17	-4.15	-3.65
H	0.00	-4.15	-3.67
COOH	0.45	-4.19	-3.78
CHO	0.42	-4.41	-3.99
CF_3	0.54	-4.33	-3.88
CN	0.66	-4.45	-4.02
NO_2	0.78	-4.47	-4.10

in energy than the HOMO of benzene. The amount by which this MO is destabilized is proportional to the electron donating strength of the substituent. For EWG's, the mechanism is different: even though the substituent would stabilize one of the degenerate HOMO's by combining it with its LUMO, this would still leave behind the other HOMO at the same energy. This level is stabilized by a σ-inductive effect that causes contraction of the π-orbitals and a lowering of their energy, including the HOMO. In the Au-BDT-Au system this causes the HOMO level to be closer to the Fermi level for EDG's and farther away from the Fermi level

for EWG's. The energy of the HOMO determines the position of the scattering state associated with it relative to the Fermi level. The position of the scattering state, in turn, determines the low bias conductance. Therefore, this is a demonstration of how adjusting the energy of a single MO in a molecule can have a direct effect on its conductance.

The resulting I-V curves are shown for all substituted BDT molecules in Fig. 4.10. As the transmission spectra predicted, a higher current can pass through the BDT molecules with EDG substituents than those with EWG substituents. Also, as predicted from the transmission spectra, NDR is predicted for all substituted BDT systems in the range between 0.2 and 0.4 V, just as for the unsubstituted BDT system.

The Hammett substituent constant σ_p is a commonly used parameter in deriving quantitative structure-activity relationships (QSAR) for a large number of chemical phenomena [85]. The σ_p values are defined from the ionization constants of benzoic acid as

$$\sigma_p = \log K_p - \log K_H, \qquad (4.2)$$

where K_H is the ionization constant for benzoic acid and K_p is the corresponding constant for the para-substituted benzoic acid. By ionization, the reaction being referred to is the removal of a proton from the COOH group in benzoic acid thus leaving behind an anion. The σ_p

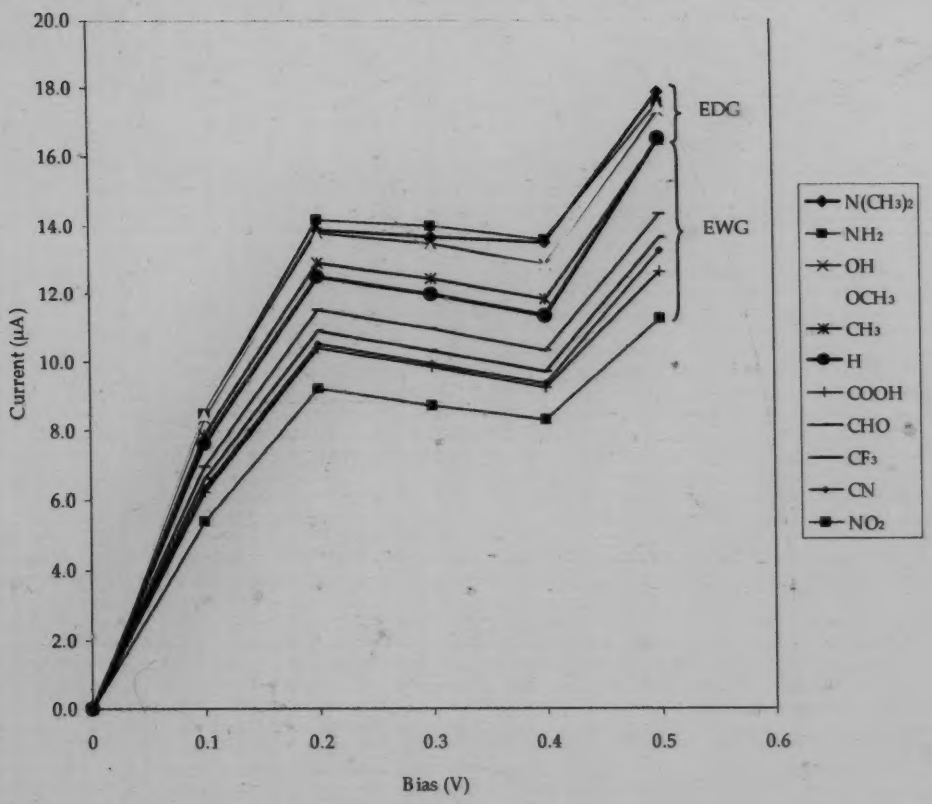

Figure 4.10. I-V characteristics for the 3x3 Au-BDT-Au system with different substituents. BDT with ED substituents has a higher current at a given bias than BDT with EW substituents.

values are therefore a measure of the ability of a substituent group to stabilize the COO^- anion from the para position on the ring. This quantity is essentially a measure of the strength of a substituent as an electron withdrawing or electron donating group [85] (see Table 4.1; EDG's are assigned negative σ_p values while EWG's are assigned positive σ_p values).

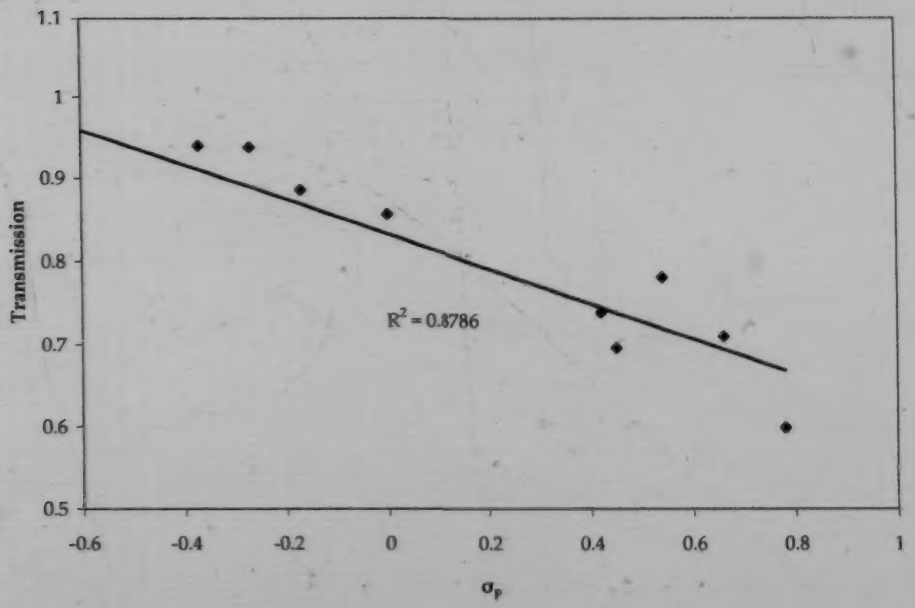

Figure 4.11. Correlation between transmission at the Fermi level for zero bias and the Hammett substituent constant σ_p [85] for the 3x3 Au-BDT-Au system.

The relation between the transmission at the Fermi level under zero bias and σ_p is shown in Fig. 4.11. The coefficient of determination (R^2) was ~0.88 suggesting a strong correlation between σ_p and the transmission. This relationship satisfies the requirement for a QSAR since it would make it possible to predetermine the transmission of a BDT molecule with a given substituent group whose c_p value is known, for this particular system.

4.4 Transport through the 5x5 Au-BDT-Au system

Similar calculations were performed on the system shown in Fig. 3.2 with the larger electrodes of 5x5 cross section. These calculations were much more computationally intensive so they were only performed for a small sample of substituted molecules to verify if the trend observed for the 3x3 electrodes was the same with the 5x5 electrodes. The three molecules studied were BDT substituted with NH_2 (EDG), H, and NO_2 (EWG). The optimized structures from Section 4.3 were used as well as the same electrode-electrode separation.

The transmission spectra for the three systems at zero bias are shown in Fig. 4.12. The energy is relative to the Fermi level for the 5x5 electrodes which was calculated to be at -3.62 eV. Recall that the Fermi level for the 3x3 electrodes was at -3.82 eV and the value for bulk Au is ca. -5.1 eV. This is a surprising result because it was expected that with larger electrodes the Fermi level would approach the bulk value, not further deviate from it. This effect remains unexplained here. In any case, the results qualitatively agree for the 5x5 electrodes with those for the 3x3 electrodes.

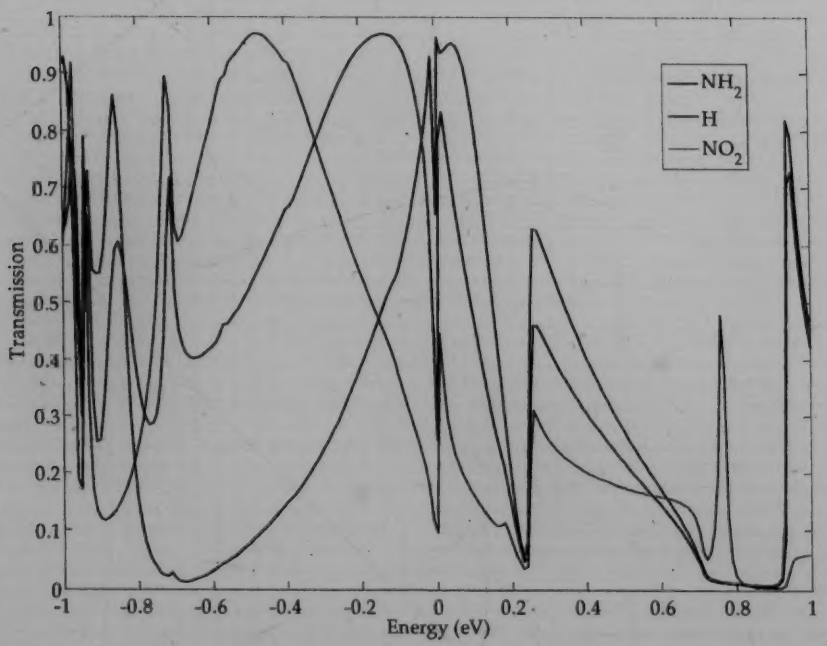

Figure 4.12. Transmission spectra for the 5x5 Au-BDT-Au system shown in Fig 3.2 with different substituents. The energy scale is relative to the Fermi level (-3.62 eV).

Just as for the 3x3 Au-BDT-Au system, the transmission at the Fermi level is higher for the BDT molecule with the EDG substituent than the unsubstituted BDT which is itself higher than the BDT molecule with the EWG substituent. A clear difference between these spectra and those obtained with the 3x3 electrodes (Fig 4.7) is the non-zero transmission in the range from -0.4 to -0.2 eV. Since the lack of transmission in this range was the source of the NDR in the systems with the 3x3 electrodes, NDR should not be observed in the 5x5 Au-BDT-Au system. Another difference

between these spectra and those obtained with the 3x3 electrodes is that in this case it is easier to see how the three systems (NH_2, H, NO_2) have similar transmission spectra with the main difference coming from the position of the large peak that is centered near 0.05 eV for NH_2, -0.15 eV for H, -0.5 eV for NO_2. This peak in the transmission spectra is once again due to transmission through the HOMO level of the molecule, as determined from a comparison of the scattering states to the MO's of the molecule. The peaks in Fig. 4.12 give a clear demonstration of how this energy level is shifted for different substituent groups and the effect this has on conductance. Since the BDT substituted with NO_2 has its HOMO level farther from the Fermi energy, it has a relatively low transmission in the vicinity of the Fermi level. Integrating under the curve around the Fermi level will result in a low current. On the other hand, the transmission is high at the Fermi level for the BDT with the NH_2 substituent so the integration under the curve will give a high current.

As for the 3x3 systems, features of the electrodes can be observed in the transmission spectra. For these systems, the transmission spectra display some sharp drops at 0 eV and at 0.25 eV. Since these coincide in energy for all three systems, they are likely due to the nature of the 5x5

electrodes just as the 3x3 Au-BDT-Au systems had low transmission for the [-0.4, -0.2] eV window.

The I-V characteristics for the three systems considered in Fig. 4.12 are shown in Fig. 4.13 along with the results of the 3x3 Au-BDT-Au systems with the same substituents for comparison. An obvious difference is the NDR for the 3x3 electrodes and lack of NDR for the 5x5 system. The ordering of the curves is the same for both the small and the large electrodes: the molecule with the NH_2 substituents has a slightly larger current than the unsubstituted BDT (H) at any given bias. The unsubstituted BDT has a relatively much higher current than the NO_2 substituted BDT at any given bias. Although the curves differ for the two types of electrodes both qualitatively (NDR) and quantitatively, they do agree in the ordering of the curves based on the substituent. An attempt to plot the three transmission values for the 5x5 systems at zero bias vs. σ_p yielded a poor linear relationship. Even though the order of the I-V plots and transmission peaks were the same, the 5x5 system does not appear to be useful as a predictive model. One reason for this may have to do with the structures used for the calculations. These were optimized as 4Au-BDT-4Au that might not fully take into account the interactions of the substituent groups (such as NO_2) and the atoms on the surface of the

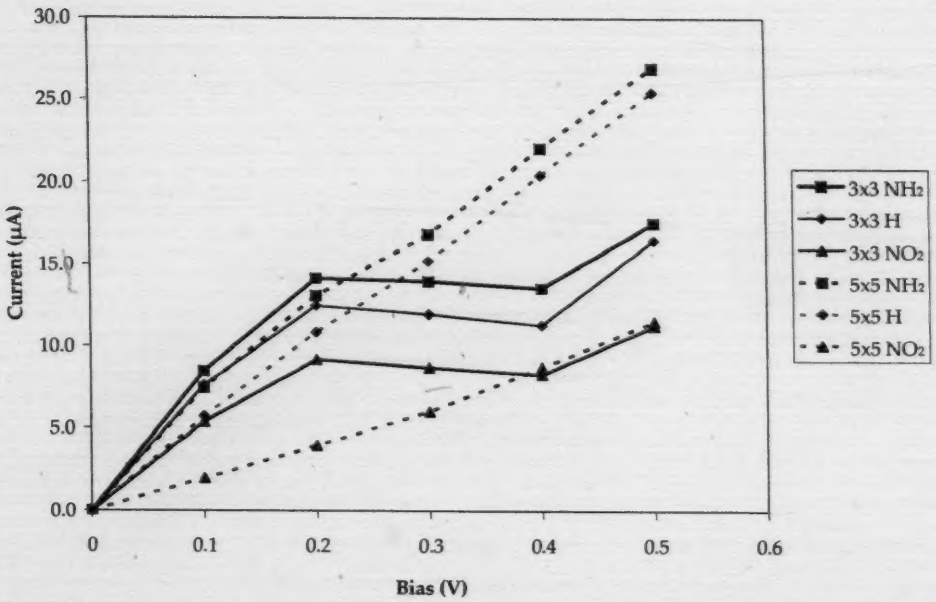

Figure 4.13. I-V comparison of current as a function of bias for three representative substituents with the small (3x3) and large (5x5) electrodes. There is no manifestation of NDR for the systems with 5x5 electrodes. The ordering of the curves is the same for the systems with both the small and large electrodes: systems with the NH_2 substituent have a slightly higher current than unsubstituted systems, which have a much higher current than systems substituted with NO_2.

electrodes. The fact that the calculated Fermi level for the 5x5 electrodes was farther away from the bulk value than the one calculated for the 3x3 electrodes may also have played a role. Another source for this discrepancy might be that the scaling of conductance with respect to the size of the electrodes may not be the same for all substituents. However,

since this is a bigger model that should offer a better representation of a real system, it seems that the results for the 3x3 systems display a fortuitous correlation with σ_p.

4.5 The substituted 3x3 Al-BDT-Al system

A previous study has shown that a molecule would conduct much better when bridging electrodes of one element over electrodes of another element [86]. In that study a naphthalene molecule was bridging electrodes made of either Au or Al by physisorbing onto the metal surface. It was found that the current in the Au-naphthalene-Au system was higher than in the Al-naphthalene-Al system. For this work, it was not only interesting to know if the current would be higher with one type of metal or another but also to see if the same trend for the current as a function of substituent group would hold. Conductance through substituted BDT molecules connected to Al (100) electrodes was studied with the aim to keep the system similar to the 3x3 Au-BDT-Au system from Section 4.3.

Figure 4.14 shows the DOS for three representative Al-BDT-Al systems including molecules containing the EDG NH_2, H, and the EWG

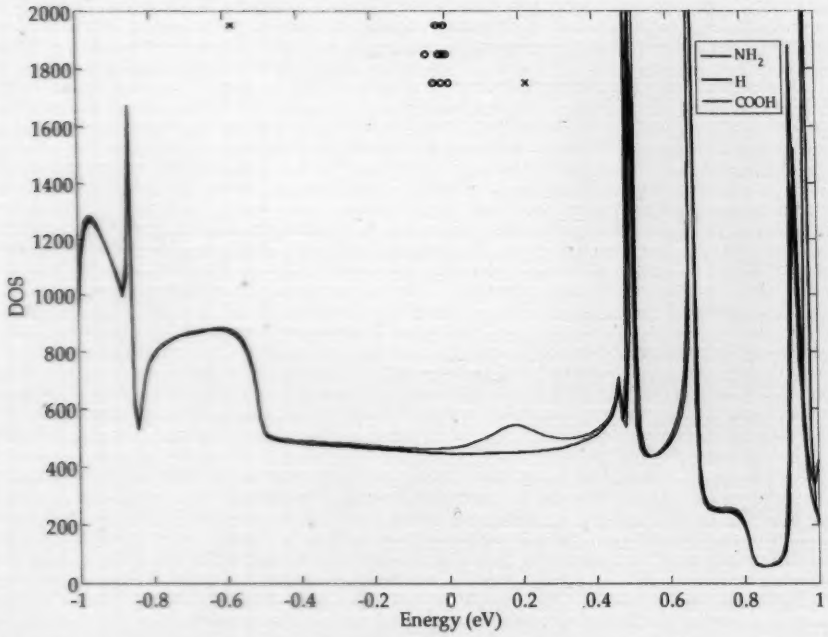

Figure 4.14. DOS for the Al-BDT-Al system for molecules with three different substituents: NH_2, H, and COOH. The relative positioning of the σ-type (o) and π-type (x) MO's of the 4Al-BDT-4Al molecule are shown at the top. The energy scale is relative to the Fermi level for Al 3x3 electrodes: -3.93 eV.

COOH substituents. The reason why the molecule with the COOH substituent was chosen for the EWG is because this molecule had the highest conductance for the Al-BDT-Al system (vide infra). The relative positions of the σ-type (o) and π-type (x) MO's that fall within the energy window for the corresponding 4Al-BDT-4Al molecules are also shown. The DOS look nearly identical for the three systems. The DOS for the

systems containing the NH_2 and H substituents are essentially indistinguishable. However, the DOS for the system containing the COOH substituent has a peak near 0.18 eV which is close to its π-type MO (LUMO+1). This feature in the DOS effectively shows the broadening of the MO. The energy scale is relative to the Fermi level of the 3x3 Al electrodes which was at -3.93 eV and the value for bulk Al is -4.3 eV. This compares much better for the Al electrodes than they did for either the 3x3 or 5x5 Au electrodes.

The resulting transmission spectra for the systems containing the EDG's and EWG's are shown in Fig 4.15. The relative positions of the MO's ('x' for π-type, 'o' for σ-type) from the isolated 4Al-BDT-4Al molecules corresponding to the systems shown in Fig. 4.14 are also included for comparison. Notice that the trend observed with Au electrodes is not present when Al electrodes are used. The molecules containing EDG's have a very low transmission compared to the molecules containing EWG's. If the transmission spectra are considered more closely, it can also be seen that even the molecules with the highest transmission peak have relatively narrow peaks which are farther away from the Fermi level when compared to those of the Au-BDT-Au system. A more subtle point is that the systems with the highest transmission peak

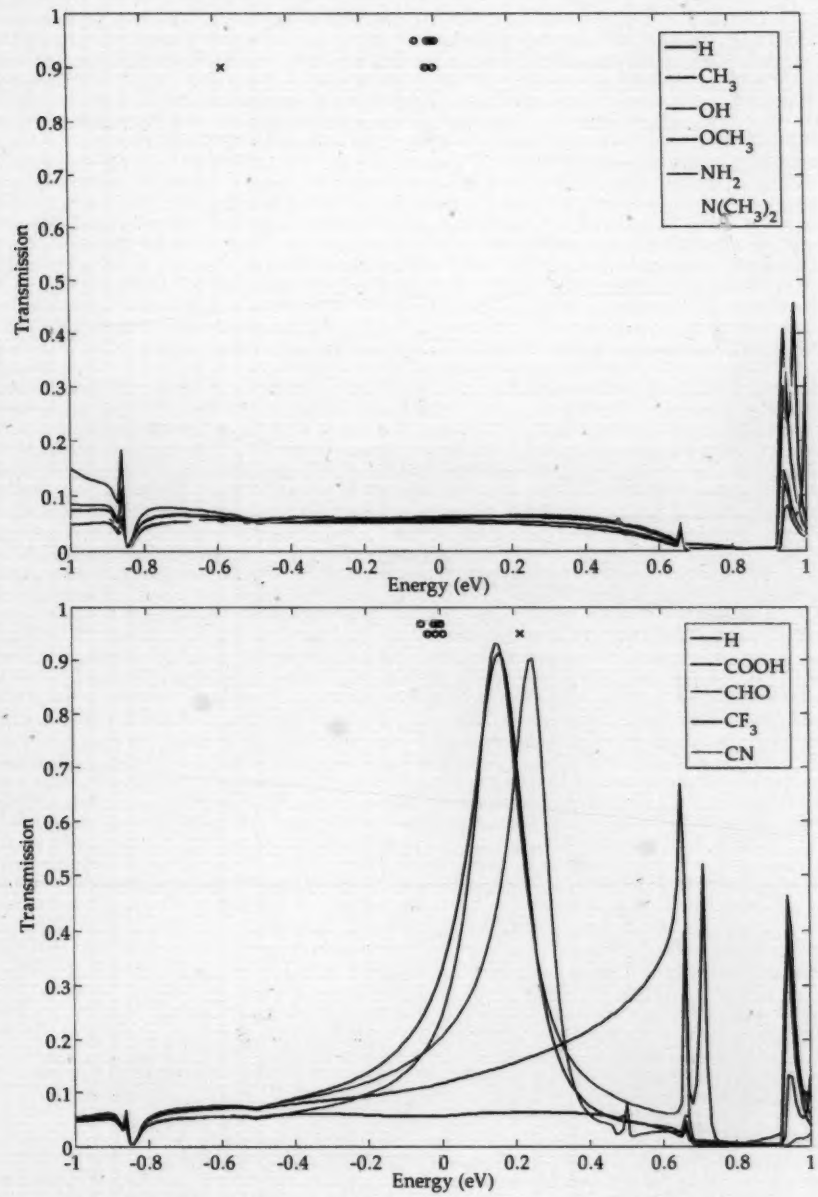

Figure 4.15. The transmission as a function of energy relative to the Fermi level (-3.92 eV) for the 3x3 Al-BDT-Al systems with different substituents on the molecule. Top: substituents are EDG's; Bottom: substituents are EWG's. The relative positions of the MO's for the NH_2, H and COOH substituted 4Al-BDT-4Al molecules are also shown: (o) for σ-type and (x) for π-type.

closest to the Fermi energy are not the systems with the strongest EWG's but systems with only weak EWG's (COOH, CHO). From the positions of the MO's and the scattering state analysis (see Fig.4.16), it was determined that the LUMO+1 contributes to the transmission peak that is observed for systems with the COOH, CHO and CN substituent groups. It is interesting to note that the LUMO+1 is a π-type MO with Al electrodes, while it is a σ-type MO with Au electrodes. This is because the MO's of the molecule will couple differently to the levels of different metals depending on their relative positions in energy. It is reasonable that the states contributing to the transmission are unoccupied MO's since the peaks are on the positive side of the Fermi level. This might explain why the EWG's have a higher transmission since they would bring the unoccupied MO's closer to the Fermi level. However it does not explain why only weakly EWG's have a relatively high conductance while strong EWG's have a low conductance. This goes to show that the way in which the MO's combine with the levels of the electrodes can result in drastic differences in the conductance behaviour from one element to another.

The current as a function of bias for the different substituents is shown in Fig. 4.17. Comparing the scales on the current axes for the 3x3 Al-BDT-Al and 3x3 Au-BDT-Au systems (Figs. 4.10 and 4.16) it is seen that

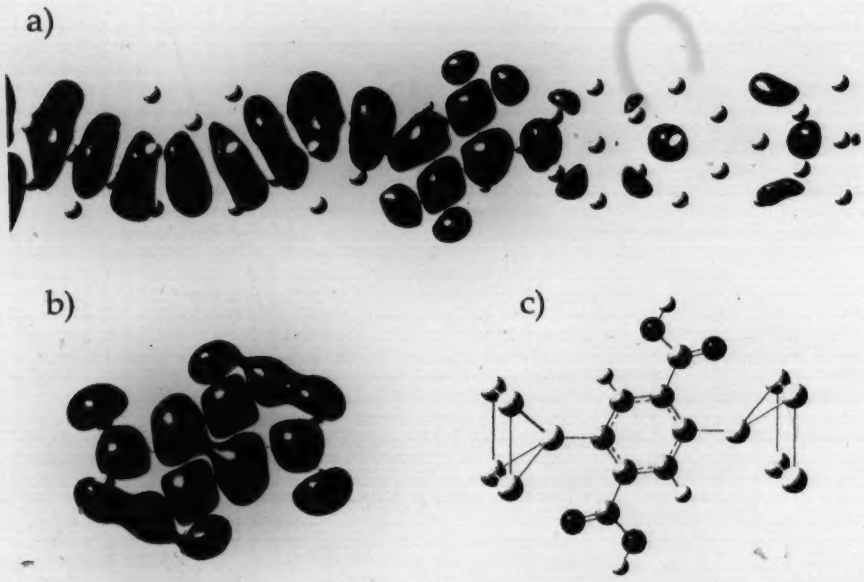

Figure 4.16. A comparison of a) the scattering state for the COOH substituted 3x3 Al-BDT-Al system in Fig. 4.15 at the peak of the transmission curve (0.16 eV) with b) the LUMO+1 of the COOH substituted 4Al-BDT-4Al molecule shown in c).

the system with Al electrodes carries about half the current at a given bias compared to the system with Au electrodes, which qualitatively agrees with another study [87], where a similar ratio was measured. As expected from the transmission spectra in Fig. 4.15, the molecules containing the EWG's COOH and CHO yield the highest current at a given bias. Based on these DFT calculations, this system also appears to have no direct relationship to the σ_p parameter and therefore could not be used as a predictive model in the same way the 3x3 Au-BDT-Au system can be.

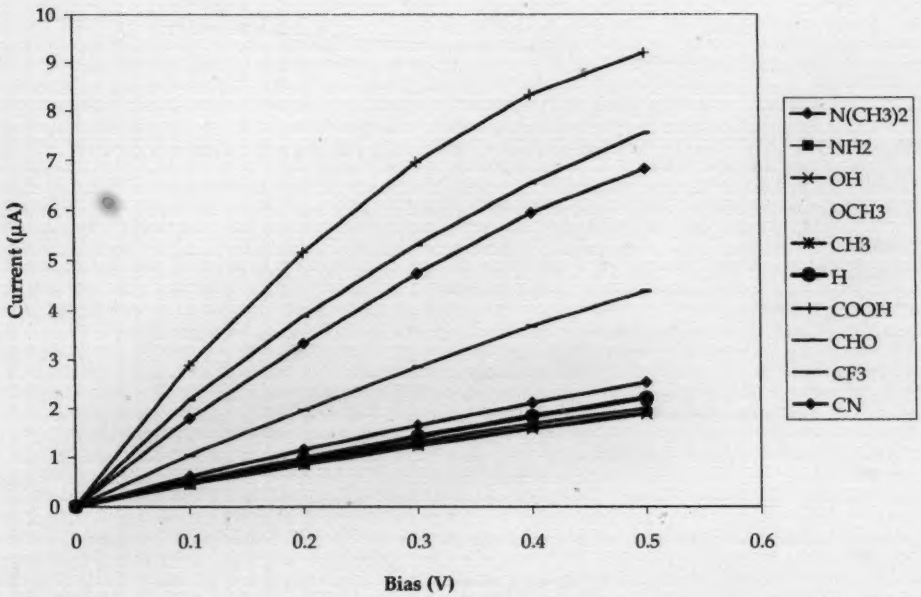

Figure 4.17. I-V plot for the 3x3 Al-BDT-Al system for BDT molecules containing different substituent groups.

Chapter 5

Conclusions

The electrical transport properties of a BDT molecule bridging two electrodes were modeled using a combination of DFT and the NEGF formalism. EDG's and EWG's were added to the BDT molecule as substituent groups in order to investigate how their electronic properties are predicted to affect the conductance. The effect of using different electrodes to connect to the BDT molecule was also investigated by comparing systems binding to the (100) face of Au electrodes with 3x3 and 5x5 cross sections as well as to the (100) face of Al electrodes with 3x3 cross section.

For the 3x3 Au-BDT-Au system, the zero bias conductance was calculated to be 66 μS which shows that the molecule in this system is a

good conductor. However this value is still two orders of magnitude higher than experiment. This level of disagreement between theory and experiment for the Au-BDT-Au system is common. The I-V characteristics of this system displayed NDR, where the current decreased with increasing bias between 0.2 and 0.4 V. This is attributed to the nature of the electrodes which did not have a continuous distribution of states as bulk Au does. It was found that adding EDG's as substituents on the BDT molecule increases its conductivity while adding EWG's decreases it. This is explained by the mode of transport at low bias which is through the HOMO of the molecule. EDG's raise the energy of the HOMO, bringing it closer to the Fermi level, while EWG's lower it, moving it farther away from the Fermi level. It was found that low bias conductance for the different substituted BDT molecules had a linear correlation to the Hammett parameter σ_p for those substituents ($R^2 = 0.88$). It is concluded that a QSAR exists which can be utilized to predict the conductance of a BDT molecule with a particular substituent based on its σ_p value.

Calculation on BDT connected to 5x5 Au electrodes showed the same qualitative trend for conductance relative to the substituent groups. However, there was no linear correlation with σ_p for this system. As for the above system, the HOMO of the BDT molecule was found responsible

for transmission at low bias. The I-V curves for this system did not show NDR, giving evidence that the effect observed for the 3x3 electrodes is due to the nature of the electrodes in combination with that of the BDT molecule.

Changing the electrodes to 3x3 Al yielded a lower conductance through the system. The same trend relating conductance to the substituents was not present for this case. The systems containing the weak EWG's gave the highest transmission. It was found that the LUMO+1 of the molecule was responsible for this transmission. Molecules with EWG's gave the highest transmission because the energy of their LUMO+1 level would be shifted closer to the Fermi level. However, the strongest EWG's have a lower transmission, and the reason for this is not known presently.

The electrical conductance behaviour through a molecule depends not only on the molecule but also on the electrodes to which it is connected. For a given molecule, if the size or composition of the electrodes is altered, the conductance can change drastically. Therefore the behaviour is not transferable from one combination of molecule and electrode to another.

Bibliography

[1] R. A. Wolkow, Annu. Rev. Phys. Chem. **50**, 413 (1999).

[2] N. S. Hush, Ann. N. Y. Acad. Sci. **1006**, 1 (2003).

[3] A. Aviram and M. A. Ratner, Chem. Phys. Lett. **29**, 277 (1974).

[4] T. Xu, I. R. Peterson, M. V. Lakshmikantham, and R. M. Metzger, Angewandte Chemie-International Edition **40**, 1749 (2001).

[5] R. M. Metzger, J. Macromol. Sci. Pure Appl. Chem. **A38**, 1499 (2001).

[6] P. G. Piva, G. A. DiLabio, J. L. Pitters, J. Zikovsky, M. Rezeq, S. Dogel, W. A. Hofer, and R. A. Wolkow, Nature **435**, 658 (2005).

[7] C. J. Muller, J. M. van Ruitenbeek, and L. J. de Jongh, Physica C **191**, 485 (1992).

[8] M. A. Reed, C. Zhou, C. J. Muller, T. P. Burgin, and J. M. Tour, Science **278**, 252 (1997).

[9] J. L. Pitters and R. A. Wolkow, Nano Lett. **6**, 390 (2006).

[10] L. Venkataraman, J. E. Klare, I. W. Tam, C. Nuckolls, M. S. Hybertsen, and M. L. Steigerwald, Nano Lett. **6**, 458 (2006).

[11] B. Xu and N. J. Tao, Science **301**, 1221 (2003).

[12] M. Büttiker, Y. Imry, R. Landauer, and S. Pinhas, Phys. Rev. B. **31**, 6207 (1985).

[13] S. Datta, *Electronic Transport in Mesoscopic Systems* (Cambridge University Press, New York, 1995).

[14] E. G. Emberley and G. Kirczenow, Phys. Rev. B. **60**, 6028 (1999).

[15] M. Brandbyge, N. Kobayashi, and M. Tsukada, Phys. Rev. B. **60**, 17064 (1999)

[16] H. Mehrez, J. Taylor, H. Guo, J. Wang, and C. Roland, Phys. Rev. Lett. **84**, 2682 (2000).

[17] C. Roland, M. B. Nardelli, J. Wang, and H. Guo, Phys. Rev. Lett. **84**, 2921 (2000).

[18] J. Taylor, Ph.D. thesis, McGill University, 2000.

[19] C. C. Wan, J.-L. Mozos, G. Taraschi, J. Wang, and H. Guo, Appl. Phys. Lett. **71**, 419 (1997).

[20] C. C. Wan, J.-L. Mozos, J. Wang, and H. Guo, Phys. Rev. B **55**, R13393 (1997).

[21] J. Wang, H. Guo, J.-L. Mozos, C. C. Wan, G. Taraschi, and Q. Zheng, Phys. Rev. Lett. **80**, 4277 (1998).

[22] G. Taraschi, J.-L. Mozos, C. C. Wan, H. Guo, and J. Wang, Phys. Rev. B **58**, 13138 (1998).

[23] W. Kohn and L. J. Sham, Phys. Rev. **140**, A1133 (1965).

[24] N. D. Lang. Phys, Rev. B **52**, 5335 (1995).

[25] N. D. Lang. Phys, Rev. B **55**, 4113 (1997).

[26] N. D. Lang and Ph. Avouris, Phys. Rev. Lett. **81**, 3515 (1998).

[27] M. Di Ventra, S. T. Pantelides, and N. D. Lang, Phys. Rev. Lett. **84**, 979 (2000).

[28] N. D. Lang and Ph. Avouris, Phys. Rev. Lett. **84**, 358 (2000).

[29] J. Taylor, H. Guo, and J. Wang, Phys. Rev. B **63**, 245407 (2001).

[30] D. Waldron, P. Haney, B. Larade, A. MacDonald, and H. Guo, Phys. Rev. Lett. **96**, 16804 (2006).

[31] X. D. Cui, A. Primak, X. Zarate, J. Tomfohr, O. F. Sankey, A. L. Moore, T. A. Moore, D. Gust, G. Harris, and S. M. Lindsay, Science **294**, 571 (2001).

[32] S. M. Lindsay and M. A. Ratner, Adv. Mater. **19**, 23 (2007).

[33] N. J. Tao, Nature Nanotechnology **1**, 173 (2006).

[34] A. Salomon, D. Cahen, S. Lindsay, J. Tomfohr, V. B. Engelkes, and C. D. Frisbie, Adv. Mater. **15**, 1881 (2003).

[35] S.-H. Ke, H. U. Baranger, and W. Yang, J. Am. Chem. Soc. **126**, 15897 (2004).

[36] H. Basch, R. Cohen, and M. A. Ratner, Nano Lett. **5**, 1668 (2005).

[37] S.-H. Ke, H. U. Baranger, and W. Yang, J. Chem. Phys. **122**, 074704 (2005).

[38] D. Q. Andrews, R. Cohen, R. P. Van Duyne, and M. A. Ratner, J. Chem. Phys. **125**, 174718 (2006).

[39] M. J. Frisch et al., Gaussian 03, Revision B.03, Gaussian, Inc., Pittsburgh, PA, 2003.

[40] A. Szabo and N. S. Ostlund, *Modern Quantum Chemistry: Introduction to Advanced Electronic Structure Theory* (Dover, Mineola, New York, 1996).

[41] P. Hohenberg and W. Kohn, Phys. Rev. **136**, B864 (1964).

[42] R. O. Jones and O. Gunnarsson, Rev. Mod. Phys. **61**, 689 (1989).

[43] K. Capelle, Braz. J. Phys. **36**, 1318 (2006).

[44] D. M. Ceperley and B. J. Alder, Phys. Rev. Lett. **45**, 566 (1980).

[45] S. Goedecker, M. Teter, and J. Hutter, Phys. Rev. B **54**, 1703 (1996).

[46] J. P. Perdew and W. Yue, Phys. Rev. B **33**, 8800 (1986).

[47] A. D. Becke, J. Chem. Phys. **98**, 5648 (1993).

[48] R. M. Martin, *Electronic Structure: Basic Theory and Practical Methods* (Cambridge Universiy Press, New York, 2004).

[49] K. S. Werpetinski and M. Cook, Phys. Rev. A **52**, R3397 (1995).

[50] J. Wang and A. A. Stuchebrukhov, Int. J. Quantum Chem. **80**, 591 (2000).

[51] N. W. Ashcroft and N. D. Mermin, *Solid-State Physics* (Thomson Learning, Toronto, 1976).

[52] M. C. Payne, M. P. Teter, D. C. Allan, T. A. Arias, and J. D. Joannopoulos, Rev. Mod. Phys. **64**, 1045 (1992).

[53] R. Landauer, IBM J. Res. Develop. **1**, 223 (1957).

[54] R. Landauer, IBM J. Res. Develop. **32**, 306 (1988).

[55] M. Büttiker, IBM J. Res. Develop. **32**, 317 (1988).

[56] M. Büttiker, Phys. Rev. B **38**, 9375 (1988).

[57] B. J. van Wees, H. van Houten, C. W. J. Beenakker, J. G. Williamson, L. P. Kouwenhoven, D. van der Marel, and C. T. Foxon, Phys. Rev. Lett. **60**, 848 (1988).

[58] J. K. Gimzewski and R. Möller, Phys. Rev. B **36**, 1284 (1987).

[59] J. M. Krans, J. M. van Ruitenbeek, V. V. Fisun, I. K. Yanson and L. J. de Jongh, Nature **375**, 767 (1995).

[60] W. Rabaud, L. Saminadayar, D. Mailly, K. Hasselbach, A. Benoit, and B. Etienne, Phys. Rev. Lett. **86**, 3124 (2001).

[61] S.-H. Ke, H. U. Baranger, and W. Yang, Phys. Rev. B **70**, 085410 (2004).

[62] L. V. Keldysh, Sov. Phys. JETP **20**, 1018 (1965).

[63] S. Datta, *Quantum Transport: Atom to Transistor* (Cambridge University Press, New York, 2005).

[64] J. Jortner, A. Nitzan, and M. A. Ratner, *Introducing Molecular Electronics*, edited by G. Cuniberti, G. Fagas, and K. Richter, (Springer-Verlay, Berling, 2005).

[65] W. Tian, S. Datta, S. Hong, R. Reifenberger, J. I. Henderson, and C. P. Kubiak, J. Chem. Phys. **109**, 2874 (1998).

[66] F. Zahid, M. Paulsson, S. Datta, "Electrical Conduction through Molecules" chapter in *Advanced Semiconductors and Organic Nano-Techniques*, edited by H. Morkoc, Academic Press 2003.

[67] M. C. Desjoqueres and D. Spanjaard, *Concepts in Surface Physics* 2nd edition (Springer-Verlag, Berlin, Heidelberg, New York, 1996).

[68] C. Lee, W. Yang, and R. G. Parr, Phys. Rev. B **37**, 785 (1988).

[69] R. B. Ross, J. M. Powers, T. Atashroo, W. C. Ermler, L. A. LaJohn, and P. A. Christiansen, J. Chem. Phys. **93**, 6654 (1990).

[70] D. R. Hamann, M. Schlüter, and C. Chiang, Phys. Rev. Lett. **43**, 1494 (1979).

[71] H. Basch and M. A. Ratner, J. Chem. Phys **123**, 234704 (2005).

[72] J. Taylor, H. Guo, and J. Wang, Phys. Rev. B **63**, 121104 (2001).

[73] Y. Xue and M. A. Ratner, Phys. Rev. B **68**, 115406 (2003).

[74] S. K. Maiti, Chem. Phys. **331**, 254 (2007).

[75] H. Chen, J. Q. Lu, J. Wu, R. Note, H. Mizuseki, and Y. Kawazoe, Phys. Rev. B **67**, 113408 (2003).

[76] X. Y. Xiao, B. Q. Xu, and N. J. Tao, Nano. Lett. **4**, 267 (2004).

[77] R. P. Andres, T. Bein, M. Dorogi, S. Feng, J. I. Henderson, C. P. Kubiak,W. Mahoney, R. G. Osifchin, and R. Reifenberger, Science **272**, 1323 (1996).

[78] M. T. Cygan, T. D. Dunbar, J. J. Arnold, L. A. Bumm, N. F. Shedlock, T. P. Burgin, L. Jones II, D. L. Allara, J. M. Tour, and P. S. Weiss, J. Am. Chem. Soc. **120**, 2721 (1998).

[79] A. Ulman, Chem. Rev. **96**, 1533 (1996).

[80] M. Brandbyge, J.-L. Mozos, P. Ordejón, J. Taylor, and K. Stokbro, Phys. Rev. B **65**, 165401 (2002).

[81] R. H. Mathews, J. P. Sage, T. C. L. G. Sollner, S. D. Calawa, C.-L. Chen, L. J. Mahoney, P. A. Maki, and K. M. Molvar, Proc. IEEE **87**, 596 (1999).

[82] C. B. Gorman, R. L. Carroll, and R. R. Fuierer, Langmuir **17**, 6923 (2001).

[83] B. Das and S. Abe, J. Phys. Chem. B **110**, 23806 (2006).

[84] G. A. DiLabio, D. A. Pratt, and J. S. Wright, J. Org. Chem. **65**, 2195 (2000).

[85] C. Hansch, A. Leo, and R. W. Taft, Chem. Rev. **91**, 165 (1991).

[86] K. Toyoda, K. Morimoto, and K. Morita, Surf. Sci. **600**, 5080 (2006).

[87] H. Sellers, A. Ulman, Y. Schnidman, and J. E. Eilers, J. Am. Chem. Soc. **115**, 9389 (1993).

Appendix A

The quantum of conductance G_0

The following is adapted from [1] and it serves the purpose of showing the origin of the quantum of conductance G_0.

A ballistic conductor with n electrons per unit of length in which the electrons move with average velocity v carries a current

$$I = env \tag{A.1}$$

where e is the charge of an electron. It is assumed that the $+k$ states in a subband are occupied by electrons moving to the right while the $-k$ states are occupied by electrons moving to the left (see Section 2.2.1). Only the $+k$ states are considered and these are populated according to some distribution function $f^+(E)$. Since the electron density associated with a

single k-state in a conductor of length L is $1/L$, the current to the right carried by a subband can be expressed as a sum over all of the populated $+k$ states as

$$I^{+} = \frac{e}{L}\sum_{k} v f^{+}(E) = \frac{e}{L}\sum_{k} \frac{1}{\hbar}\frac{\partial E}{\partial k} f^{+}(E) \tag{A.2}$$

where the velocity can also be expressed as the first derivative of the dispersion relation $E(k)$ with respect to k, divided by $\hbar$. If periodic conditions are assumed, the summation over k can be converted into an integral as

$$\sum_{k} \rightarrow 2\times\frac{L}{2\pi}\int dk \tag{A.3}$$

where the factor of 2 is added for spin, and

$$I^{+} = \frac{2e}{h}\int_{-\infty}^{\infty} f^{+}(E)dE \tag{A.4}$$

is obtained. If this integration is carried out over a range of energies from μ_1 to μ_2 in which $f^{+}(E) = 1$, the current to the right becomes

$$I^{+} = \frac{2e}{h}\int_{\mu_1}^{\mu_2} f^{+}(E)dE = \frac{2e^2}{h}\left(\frac{\mu_2 - \mu_1}{e}\right) = G_0 V \tag{A.5}$$

which shows the origin of G_0 ($\approx 77\mu S$).

[1] N. W. Ashcroft and N. D. Mermin, *Solid-State Physics* (Thomson Learning, Toronto, 1976).

Appendix B

Surface Green's function

Since a semi-infinite electrode is periodic in the z-direction, its Hamiltonian can be expressed as an infinitely large block-tridiagonal matrix

$$\hat{H} = \begin{pmatrix} h_s & h_1 & & & & \\ h_2 & h_0 & h_1 & & & \\ & h_2 & h_0 & h_1 & & \\ & & h_2 & h_0 & h_1 & \\ & & & h_2 & h_0 & \ddots \\ & & & & \ddots & \ddots \end{pmatrix} \tag{B.1}$$

where h_0 is the Hamiltonian for an arbitrary repeating cell; and h_1 and h_2 are overlap matrices between neighbouring cells. It is assumed that there is no direct coupling between second neighbouring cells, which is a fair assumption supposing the cells are chosen to be large enough (however

there might be indirect coupling). h_s is taken to be the cell that will be connected to the central (scattering) region and it is the focus of attention. Letting G be the inverse of $\hat{H}$, where G will generally not be block-tridiagonal, the first diagonal block of G is of interest,

$$g_s \equiv G_{00} = (\hat{H}^{-1})_{00} \tag{B.2}$$

because it represents the surface Green's function g_s that is sought after from $\hat{H}$ (see Section 2.3.3). Note that the indices start from 0.

Two approaches that are used to solve this problem include a Bloch wave method [1] and an iteration method [2]. The latter is presented here since it is the one implemented in the MATDCAL package [3].

By starting out with only the first column of G, where $g_i = G_{i0}$ is defined, and multiplying it by $\hat{H}$

$$\begin{pmatrix} h_s & h_1 & & \\ h_2 & h_0 & h_1 & \\ & h_2 & h_0 & \ddots \\ & & \ddots & \ddots \end{pmatrix} \begin{pmatrix} g_0 \\ g_1 \\ g_2 \\ \vdots \end{pmatrix} = \begin{pmatrix} 1 \\ 0 \\ 0 \\ \vdots \end{pmatrix} \tag{B.3}$$

is obtained from the inverse relationship. The equation for the first row yields the relationship

$$h_s g_0 = 1 - h_1 g_1 \tag{B.4}$$

and for all other rows

$$h_2 g_{n-1} + h_0 g_n + h_1 g_{n+1} = 0 \qquad (n \geq 1) \tag{B.5}$$

Rearranging Eq. (B.5),

$$g_n = t_0 g_{n-1} + \tilde{t}_0 g_{n+1} \quad (n \geq 1),$$

$$t_0 = -h_0^{-1} h_2, \tag{B.6}$$

$$\tilde{t}_0 = -h_0^{-1} h_1.$$

Applying this relation to g_{n-1} and g_{n+1}, the recursive relation can be derived for next nearest neighbours

$$g_n = t_1 g_{n-2} + \tilde{t}_1 g_{n+2} \quad (n \geq 2),$$

$$t_1 = -(1 - t_0 \tilde{t}_0 - \tilde{t}_0 t_0)^{-1} t_0^2, \tag{B.7}$$

$$\tilde{t}_1 = -(1 - t_0 \tilde{t}_0 - \tilde{t}_0 t_0)^{-1} \tilde{t}_0^2.$$

Repeating the above step will give

$$g_n = t_l g_{n-2^l} + \tilde{t}_l g_{n+2^l} \quad (n \geq 2^l)$$

$$t_l = -(1 - t_{l-1} \tilde{t}_{l-1} - \tilde{t}_{l-1} t_{l-1})^{-1} t_{l-1}^2 \tag{B.8}$$

$$\tilde{t}_l = -(1 - t_{l-1} \tilde{t}_{l-1} - \tilde{t}_{l-1} t_{l-1})^{-1} \tilde{t}_{l-1}^2$$

on the l^{th} iteration. From Eq. (B.8),

$$g_1 = t_0 g_0 + \tilde{t}_0 g_2,$$

$$g_2 = t_1 g_0 + \tilde{t}_1 g_4, \tag{B.9}$$

$$\cdots$$

$$g_{2^l} = t_l g_0 + \tilde{t}_l g_{2^{l+1}},$$

can be obtained. Consecutive substitutions into Eq. (B.9) will yield

$$g_1 = T_l g_0 + S_l g_{2^{l+1}},$$

$$T_l = t_0 + \tilde{t}_0 t_1 + \tilde{t}_0 \tilde{t}_1 t_2 + \tilde{t}_0 \tilde{t}_1 \tilde{t}_2 \ldots \tilde{t}_{l-1} t_l, \qquad \text{(B.10)}$$

$$S_l = \tilde{t}_0 \tilde{t}_1 \tilde{t}_2 \cdots \tilde{t}_{l-1} \tilde{t}_l .$$

For sufficiently large l, the term $g_{2^{l+1}}$ becomes very small and can be neglected [2] so that

$$g_1 = T_l g_0, \qquad \text{(B.11)}$$

into which Eq. (B.4) can be substituted in order to get the relation for the surface Green's function

$$\boxed{g_s = g_0 = (h_s + h_1 T)^{-1}}. \qquad \text{(B.12)}$$

[1] S. Sanvito, C. J. Lambert, J. H. Jefferson, and A. M. Bratkovsky, Phys. Rev. B **59**, 11936 (1999).

[2] M. P. Lopez Sancho, J. M. Lopez Sancho, and J. Rubio, J. Phys. F: Met. Phys. **14**, 1205 (1984).

[3] D. Waldron, P. Haney, B. Larade, A. MacDonald, and H. Guo. Phys. Rev. Lett. **96**, 16804 (2006).